Use of Digital Image Analysis For Studies of Renal Physiology

Edward J. Delp

Video and Image Processing Laboratory (VIPER)

School of Electrical and Computer Engineering

School of Biomedical Engineering

Purdue University

West Lafayette, Indiana

Acknowledgement

Our Team

- **Kenneth Dunn – IU - Indiana Center for Biological Microscopy**
- **Paul Salama – Department of Electrical and Computer Engineering – IUPUI**
- **Seth Winfree - IU - Indiana Center for Biological Microscopy**

- **Graduates Students (current and former) – Kevin Lorenz, Neeraj Gadgil, Soonam Lee, David Ho, Chichen Fu, and Shuo Han**

Acknowledgement

- **This work was supported by a George M. O'Brien Award from the National Institutes of Health NIH/NIDDK P30 DK079312 and the endowment of the Charles William Harrison Distinguished Professorship at Purdue University**

Our Project Goals

- **Develop tools for microscopy image analysis and visualization – e.g. registration, segmentation, nuclei detection**
- **Develop methods based on the latest approaches in image analysis and computer vision**
- **Develop tools that are "biologist aware" ➔ semi-automatic approaches may be better than fully automatic methods**

Motivation

- **Fluorescence microscopy is a form of optical microscopy used to image/visualize subcellular structures in living cells or animals**
- **"Fluorescence" is the emission of light by the process of absorbing and releasing energy from fluorescent molecules**

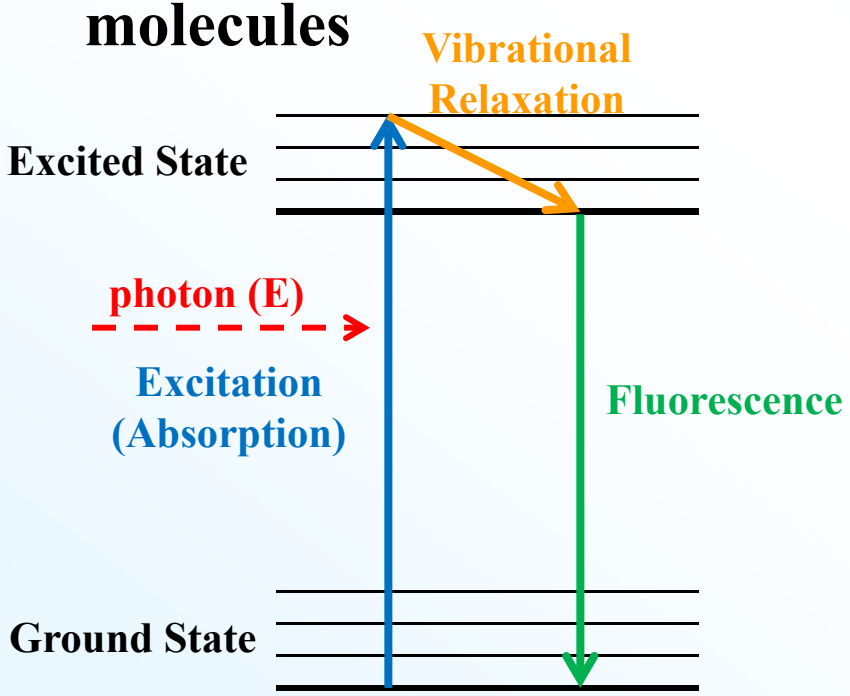

Jablonski diagram

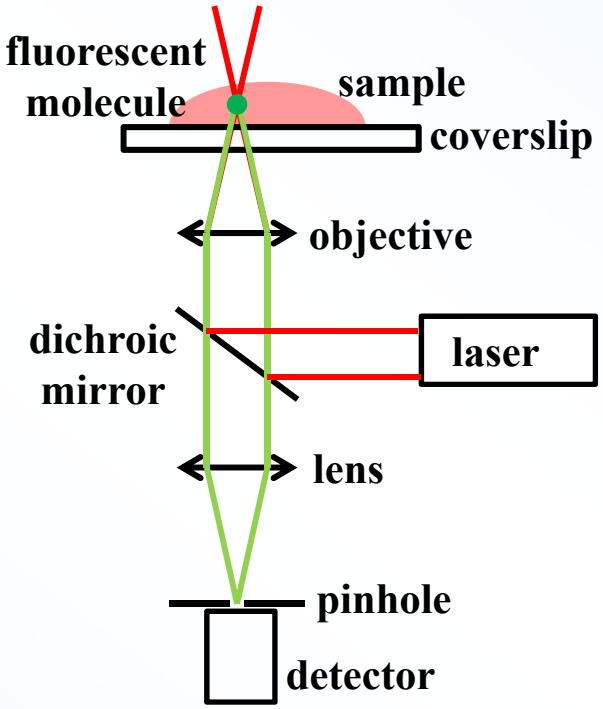

Confocal microscopy

Motivation

- The energy of a photon is inversely proportional to the wavelength

$$E = \frac{hc}{\lambda}$$

- Confocal microscopy uses light with shorter wavelengths
- Two-photon microscopy simultaneously excites fluorescent molecules with longer wavelengths
- Two-photon microscopy enables image/visualize in deeper tissue

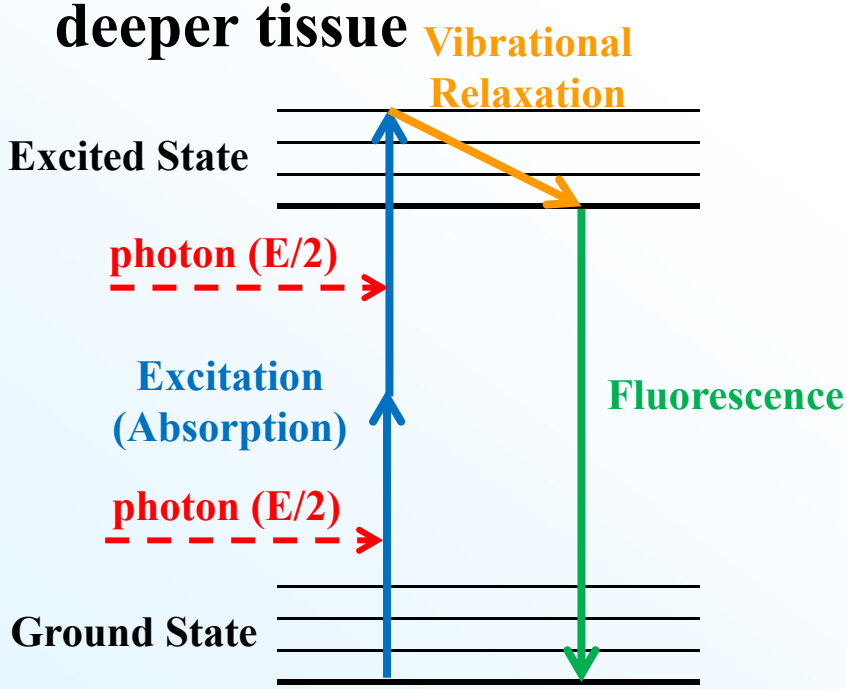

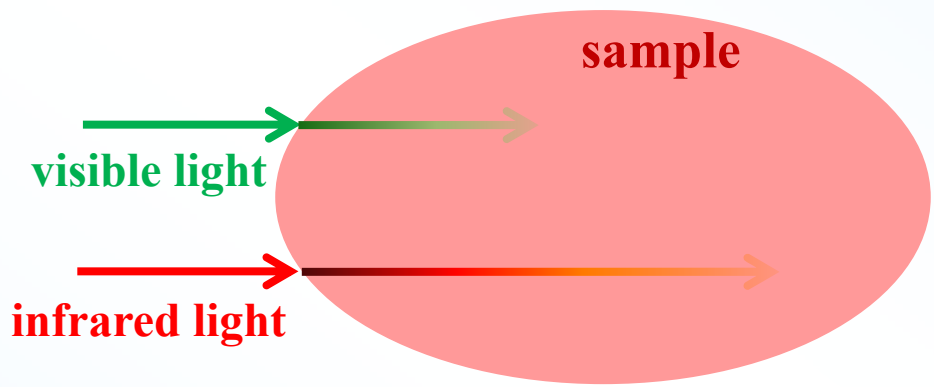

Image Data Volumes

- **Two types of multiphoton microscopy image sets:**
  - **Three dimensional / volumetric / Z-series (progressively increasing tissue depths)**
  - **Time-series (progressively increasing time instances for single or multiple focal planes)**

- **Single-channel or multi-channel data sets**

Challenges

- **Image contrast decreases with depth in biological tissues due to increased light scattering and absorption**
- **Image resolution (spatial and temporal) and signal levels are decreased due to the need for high image capture rates necessary to image dynamic biological structures**
- **Segmentation results are very sensitive to small changes in parameters, causing the failure of typical image analysis/computer vision methods**
- **Objects have poorly defined edges (sparse, not rigid and continuous)**

Challenges

- **So type automatic image analysis is necessary (size and complexity of image volumes make manual image analysis impractical) – lack of ground truth data**
- **Image sets are frequently obtained from live specimens – motion artifacts are introduced from respiration and heartbeat**
- **Data sets is corrupted with noise from a variety of sources and distributions**

Challenges – Channel Crosstalk

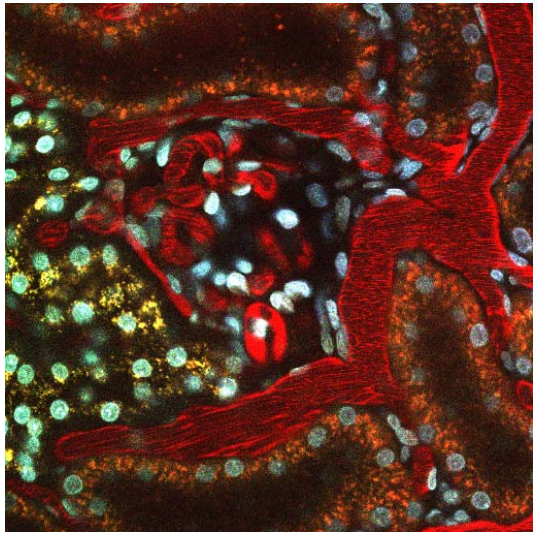

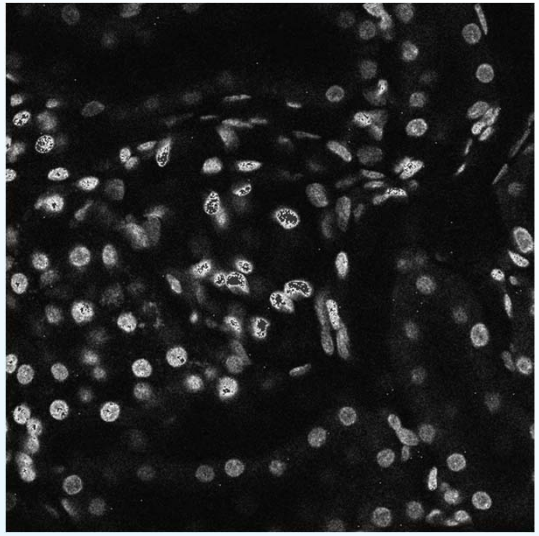

Blue

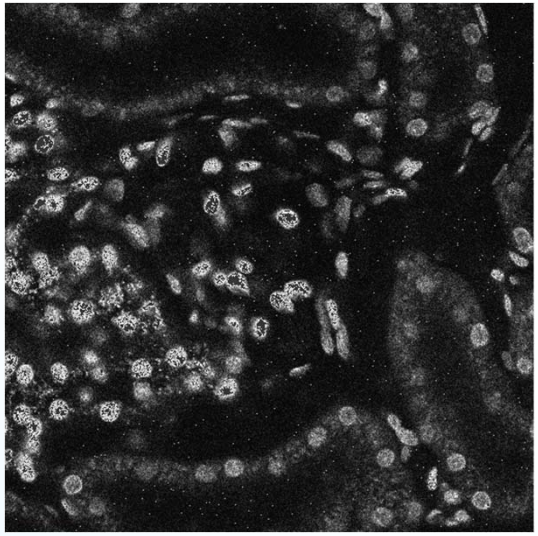

Green

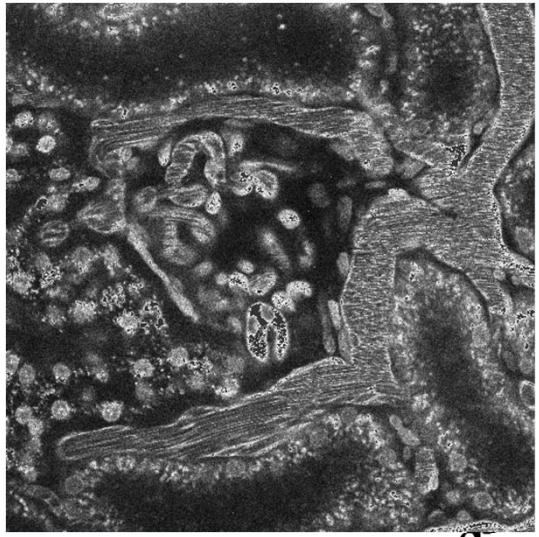

Red

Notation

I_{z_p,t_q,c_r} represents our images whose size is $X \times Y$ where z_p, t_q, c_r represents P focal slices, Q time samples, and R spectral channels where

$$p \in \{1,\cdots,P\} \quad q \in \{1,\cdots,Q\} \quad r \in \{1,\cdots,R\}$$

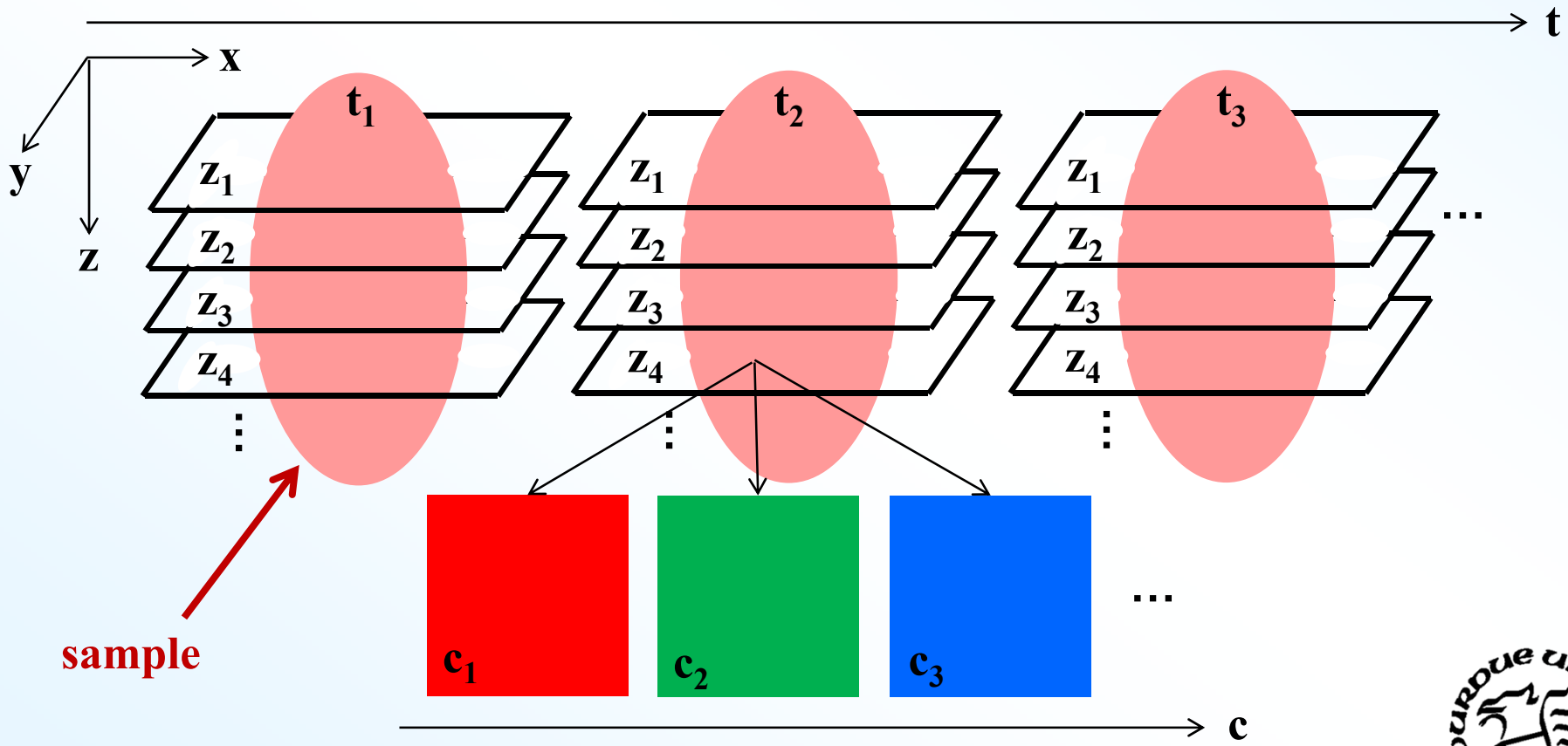

4D Image Registration

Acknowledgement

- **The images used in this method for microscopy image registration were provided by Dr. Martin Oberbarnscheidt of the University of Pittsburgh and the Thomas E. Starzl Transplantation Institute**

Research Goal

- **4D immune cells taken from live rat kidney using two-photon microscopy**
  - **X = 512, Y = 512, P = 11, Q = 61, R = 4**
- **Motion artifacts are generated during the data acquisition process due to animal's heart beating and respiration**
- **The goal is to minimize motion artifact both in the z direction and in time**

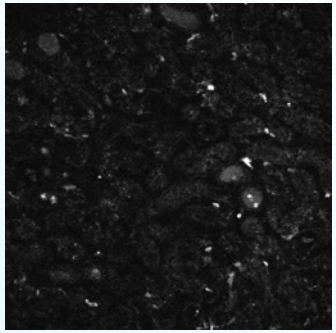

$F_{z_6t_1c_1}$

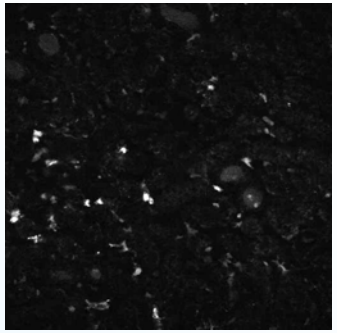

$F_{z_6t_1c_2}$

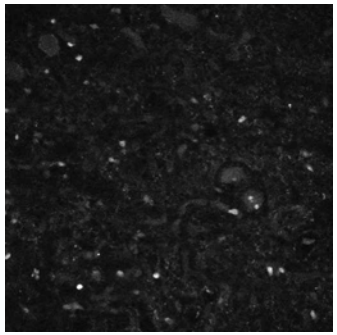

$F_{z_6t_1c_3}$

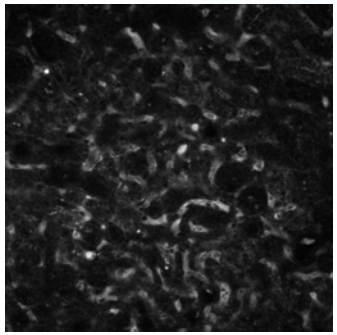

$F_{z_6t_1c_4}$

Proposed Method

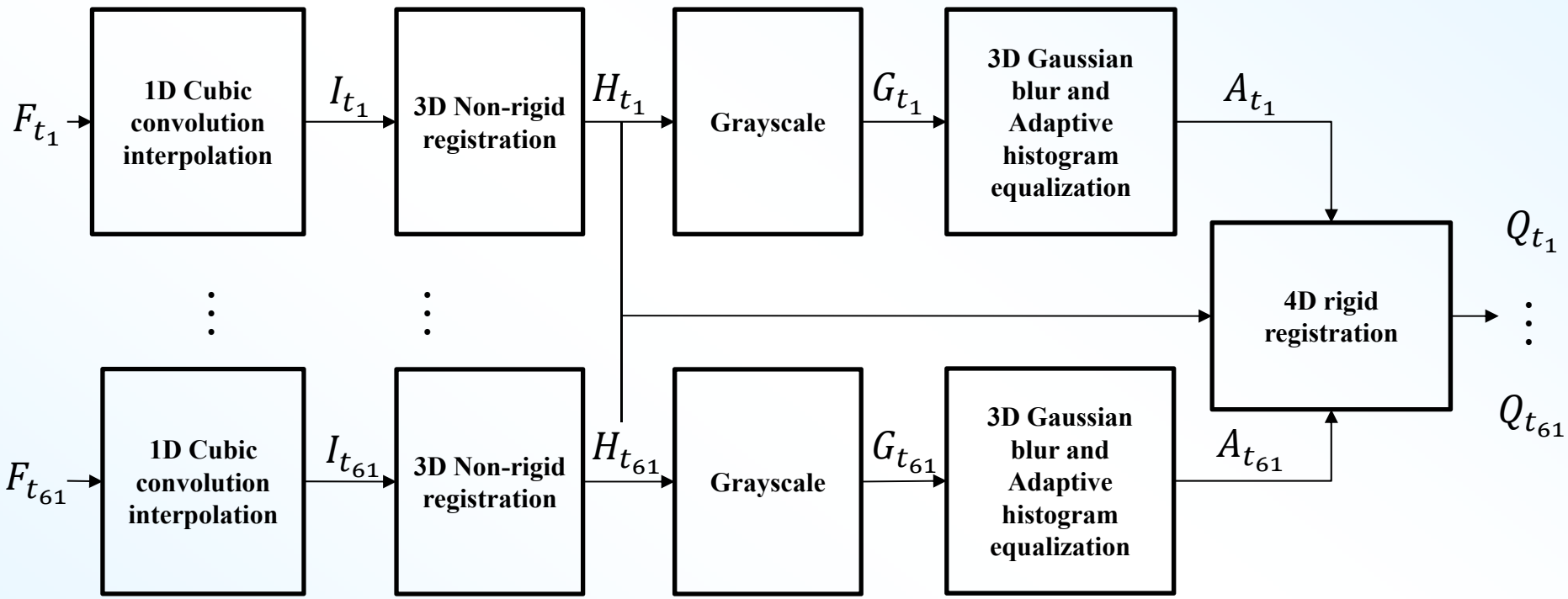

1D Interpolation

- **1D cubic convolution interpolation in Z direction to smooth the images**
- **After this process, the number of images in the z direction is increased from 11 to 41**

Original z section image

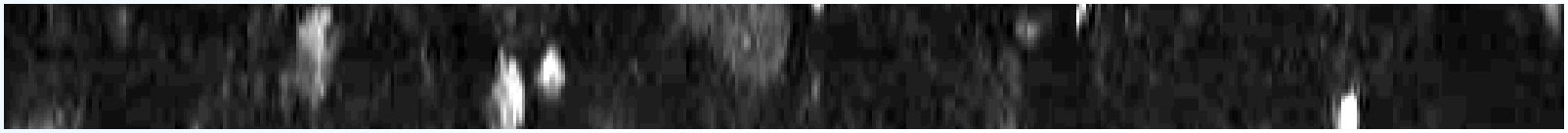

Interpolated z section image

3D B-Splines Non-Rigid Registration

- Images in the z direction are acquired serially
- Motion artifacts between images slices in z direction need to be removed
- Our 3D non-rigid registration technique is used on each 3D volume to remove the motion artifacts

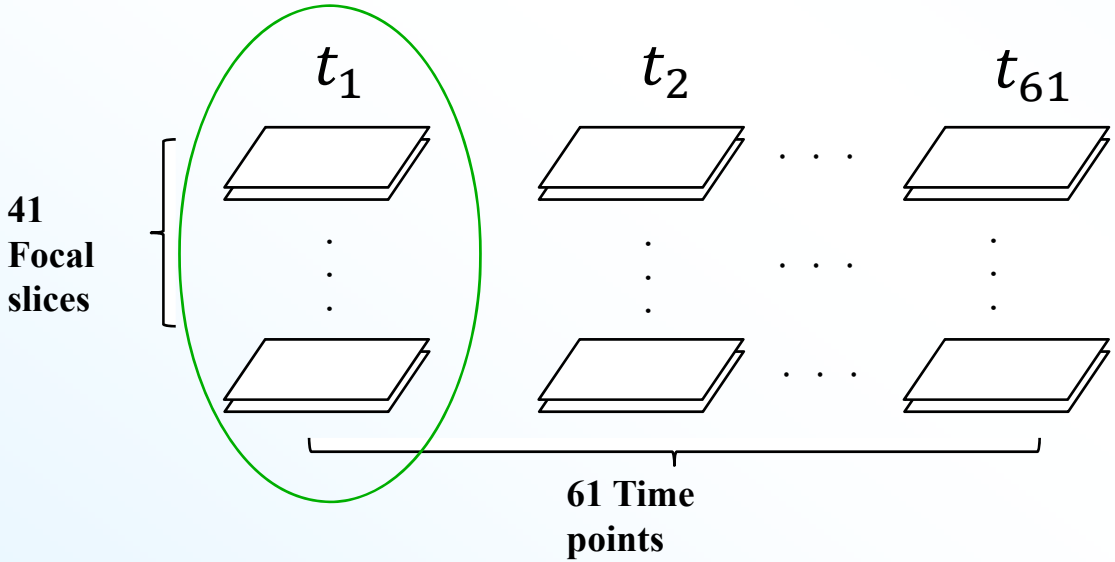

3D Non-Rigid Registration

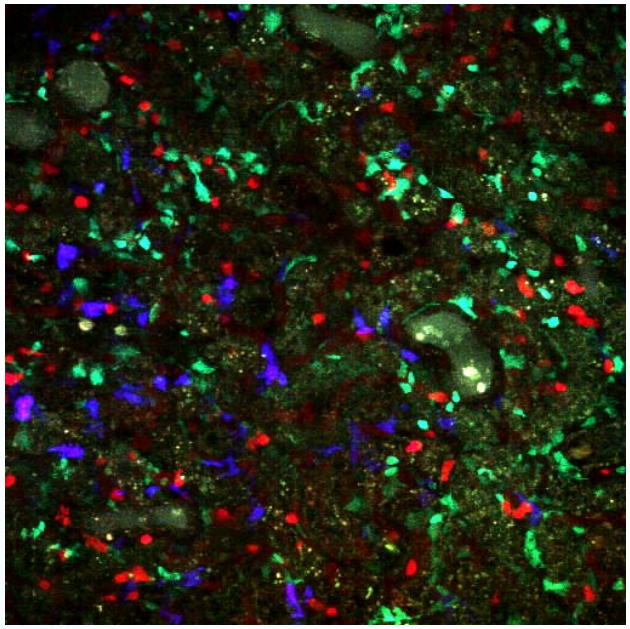

Original image XY

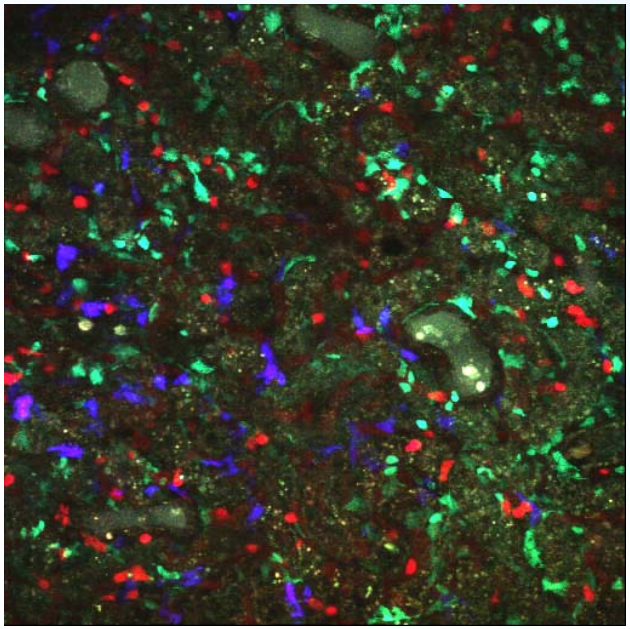

Registered image XY

Original image YZ

Registered image YZ

Proposed Method

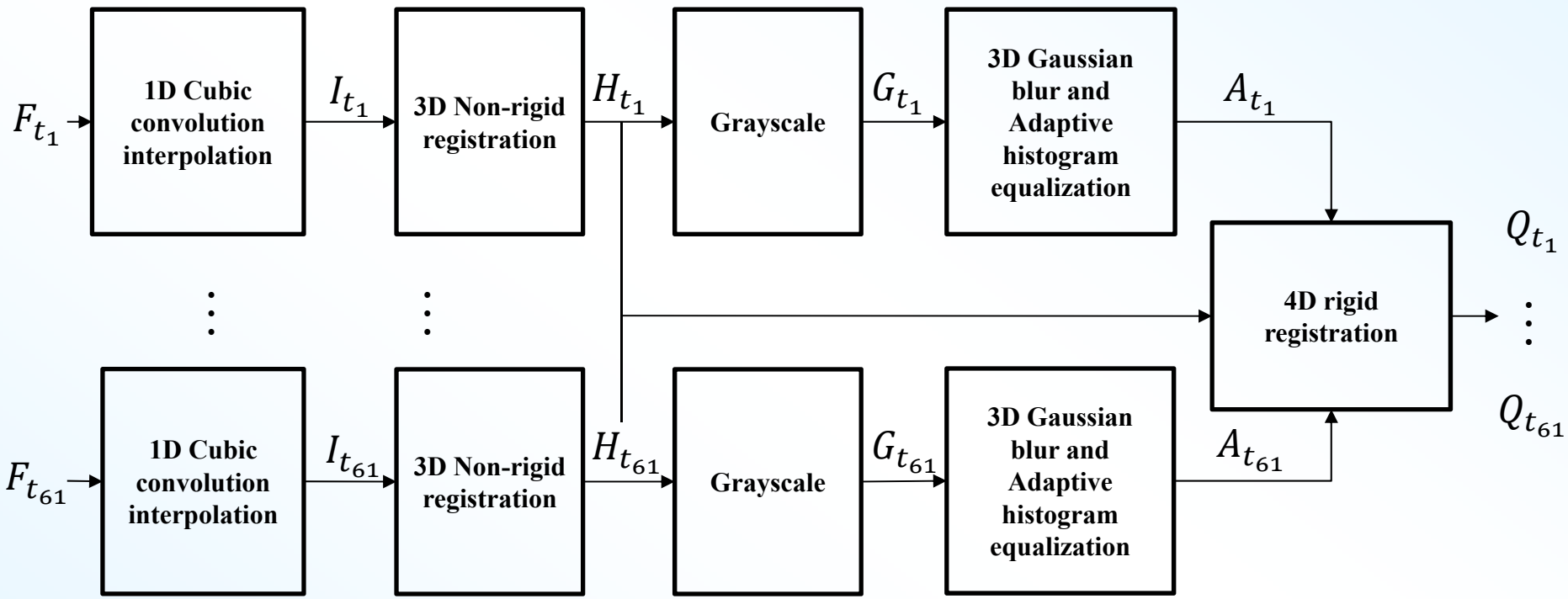

3D Gaussian Blur and Adaptive Histogram Equalization

- **3D Gaussian blur and adaptive histogram equalization (AHE) are used to create better defined biological structures in our images**
  - **A rectangular window with size of 17 ×17×9 is used in 3D Gaussian blur**
  - **Adaptive histogram equalization employs a rectangular window with size of 17 ×17×9**

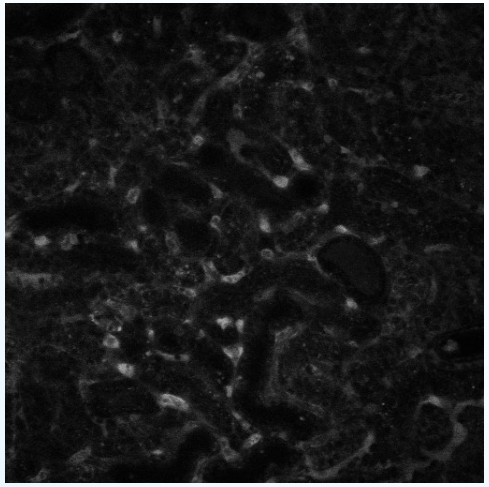

Original

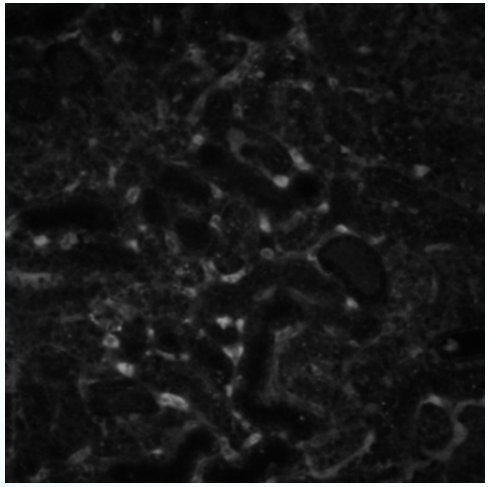

Gaussian blur

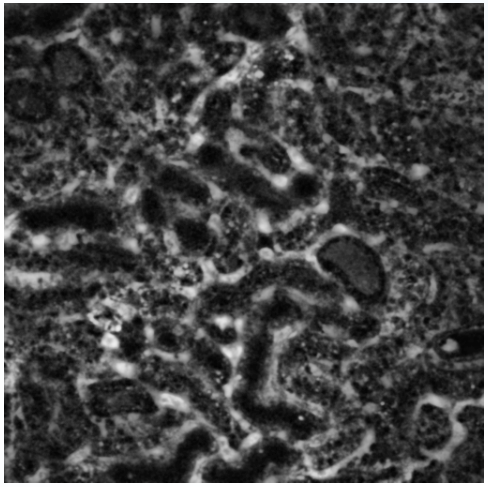

AHE

4D Rigid Registration

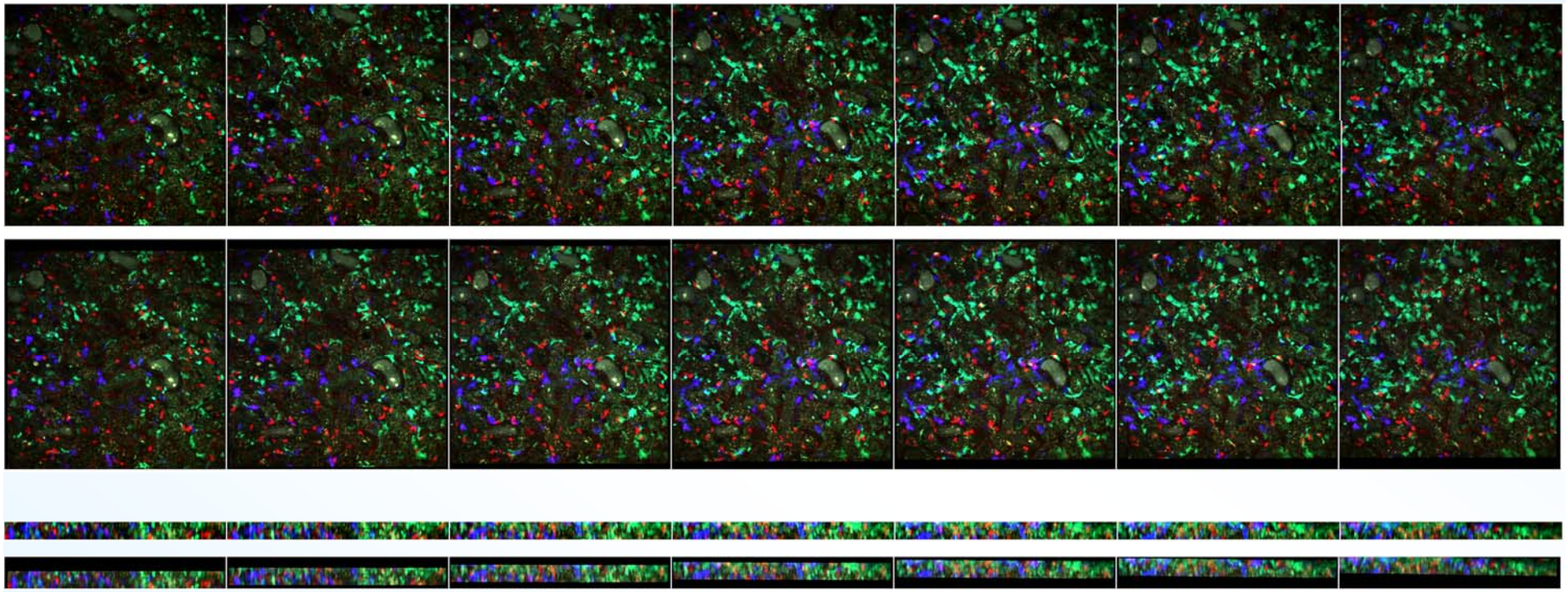

7 sample time points in XY and YZ views

Results

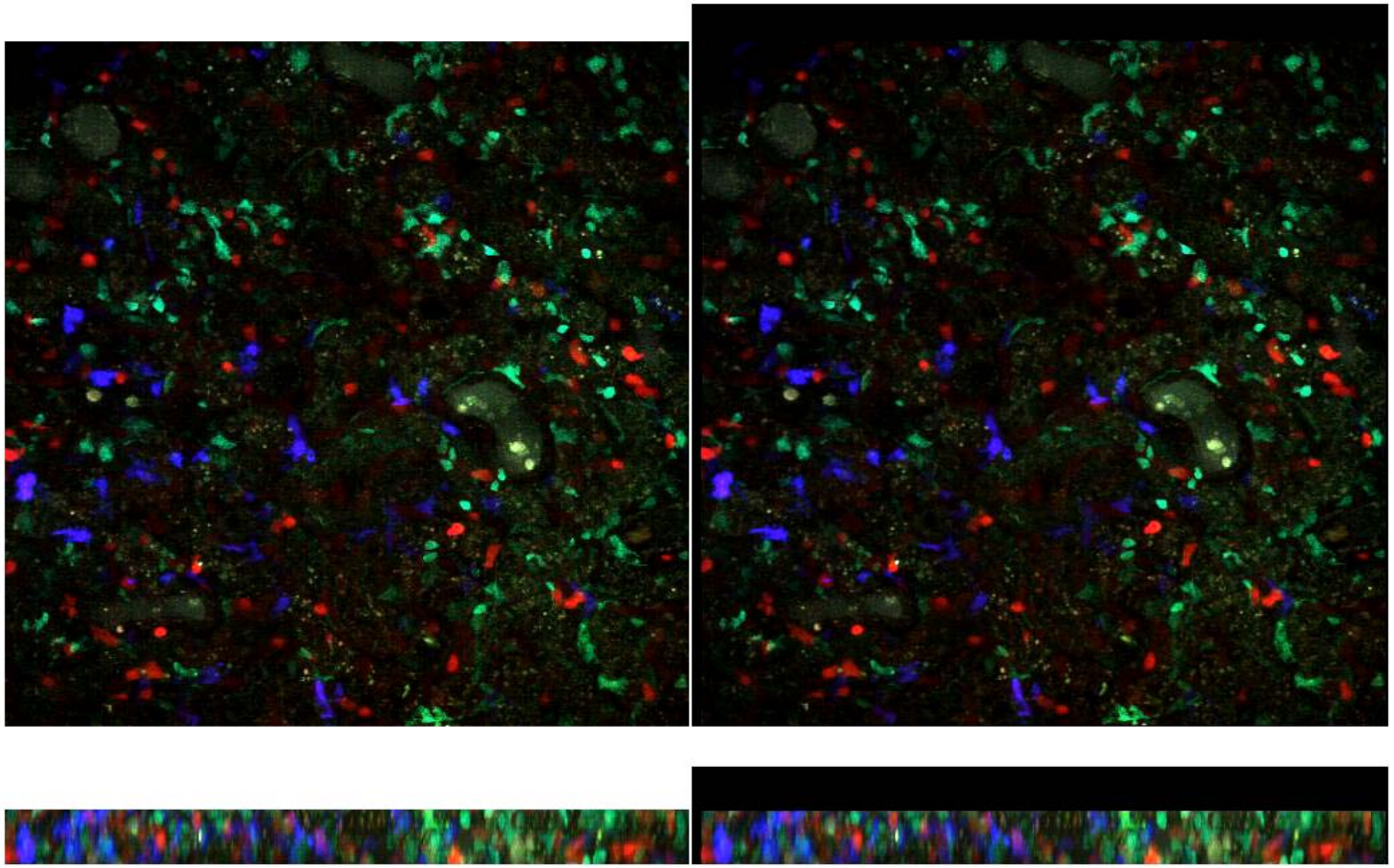

Validation

MIP of XY

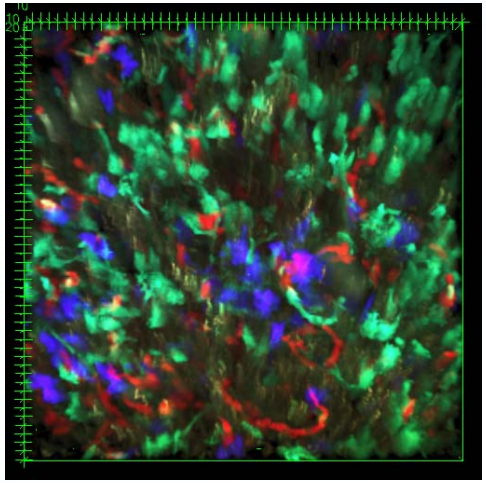

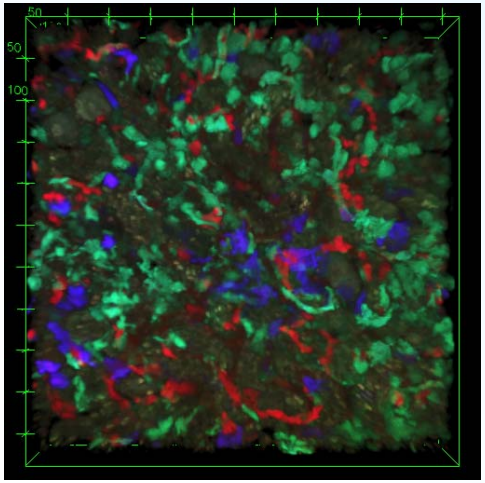

MIP of YZ

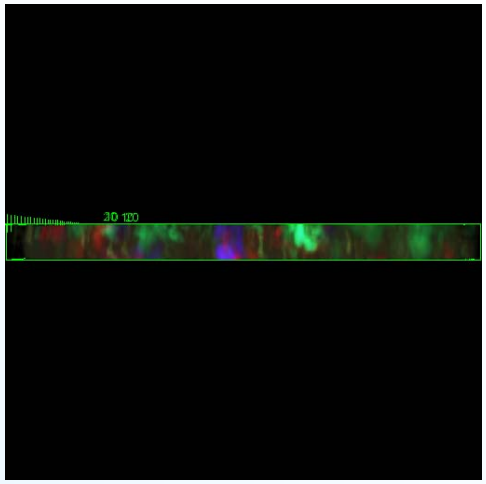

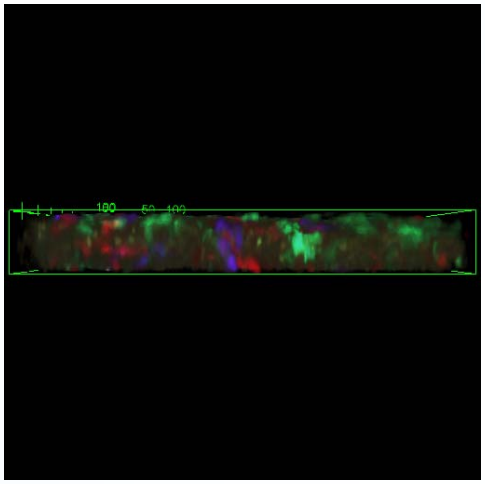

* Maximum Intensity Projection (MIP)

Original **Registered**

3D Spherical Histograms of Motion Vectors

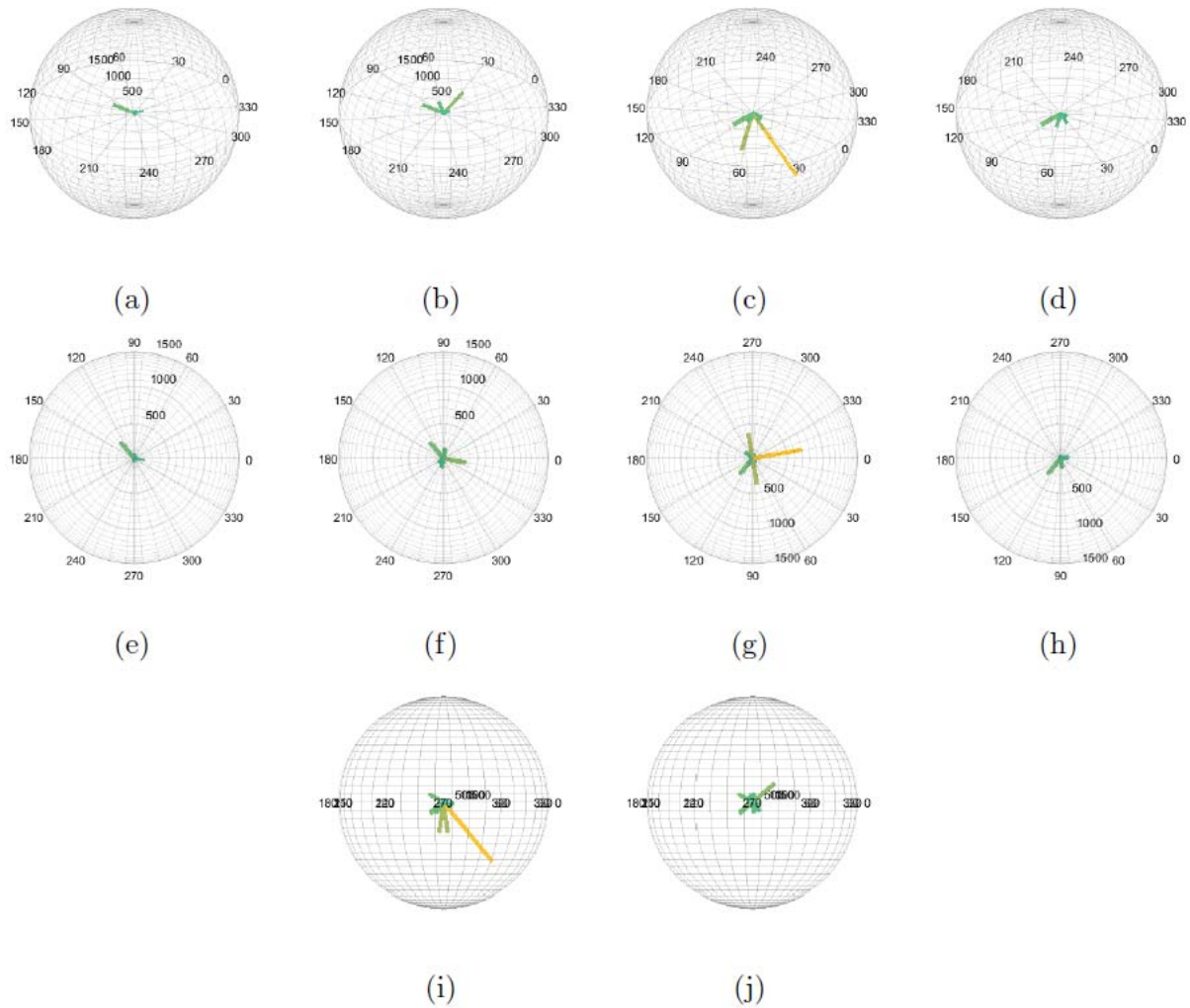

(a) histogram of original volume in the view from top,
(b) histogram of registered volume in the view from top,
(c) histogram of original volume in the view from bottom,
(d) histogram of registered volume in the view from bottom,
(e) histogram of original volume in +XY view,
(f) histogram of registered volume in +XY view,
(g) histogram of original volume in -XY view,
(h) histogram of registered volume in -XY view,
(i) histogram of original volume in XZ view,
(j) histogram of registered volume in XZ view.

Nuclei Segmentation

Marked Point Process (MPP) + Midpoint Analysis

Nuclei Segmentation: Our Proposed Method

Original Blue Channel Image

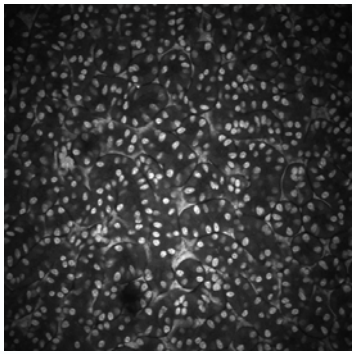

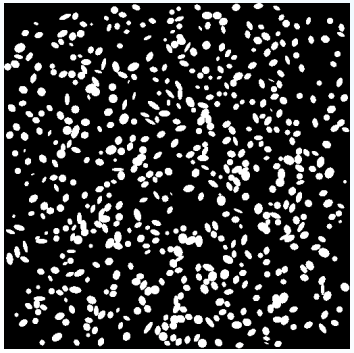

Segmentation Result

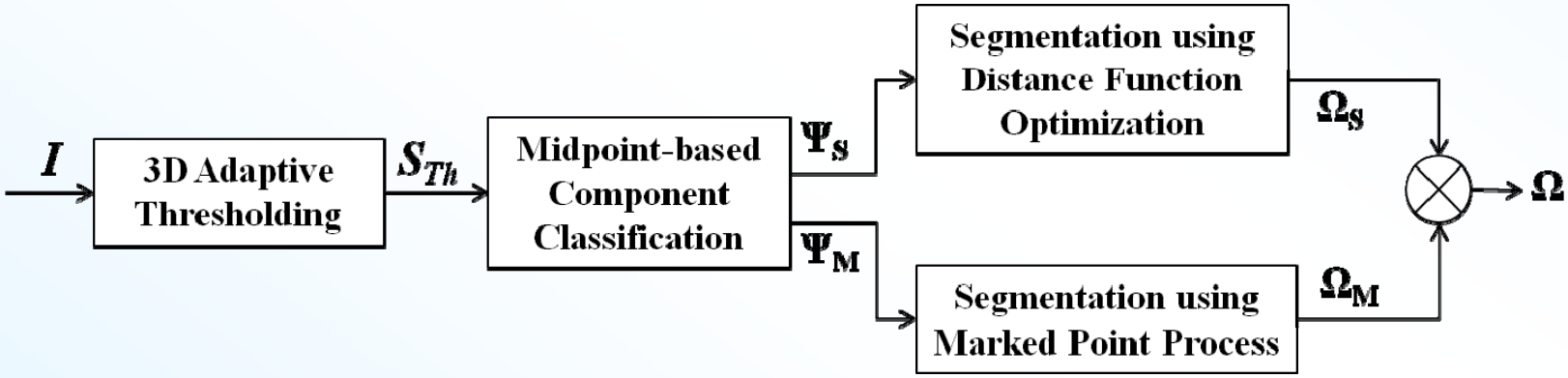

Block Diagram

Adaptive Thresholding

Goal: To separate foreground that represents biological entity

Let $I(t) \in [0,1]$ **be the pixel intensity at pixel** t **of the image**

Thresholding function (Use local 3D information)

$$f_{Th} : [0,1] \rightarrow [-1,1] \qquad f_{Th}(t) = \begin{cases} \dfrac{I(t)-(\tau_t+\tau_c)}{1-(\tau_t+\tau_c)} & \textbf{if} \quad I(t) \geq (\tau_t+\tau_c) \\ -\dfrac{(\tau_t+\tau_c)-I(t)}{(\tau_t+\tau_c)} & \textbf{if} \quad I(t) < (\tau_t+\tau_c) \end{cases}$$

τ_t **: Mean pixel intensity of the window** $(w_{Th,x} \times w_{Th,y} \times w_{Th,z})$ **at** t

τ_c **: A positive constant used as a fixed additive threshold**

Voting function (Aggregate votes) $f_v : [-1,1] \rightarrow (-\infty, \infty)$

$$f_v(t) = (f_{Th} * g_v)(t) \qquad g_v(x,y,z) = e^{-\frac{|x|^2+|y|^2+|z|^2}{a^2}}$$ **for window** $(w_{v,x} \times w_{v,y} \times w_{v,z})$ **at** t

Foreground Mask $S_M = \{t : f_v(t) \geq 0\}$

Midpoint Analysis

Goal: To classify each connected component as

(i) single-object component (ii) multiple-object component

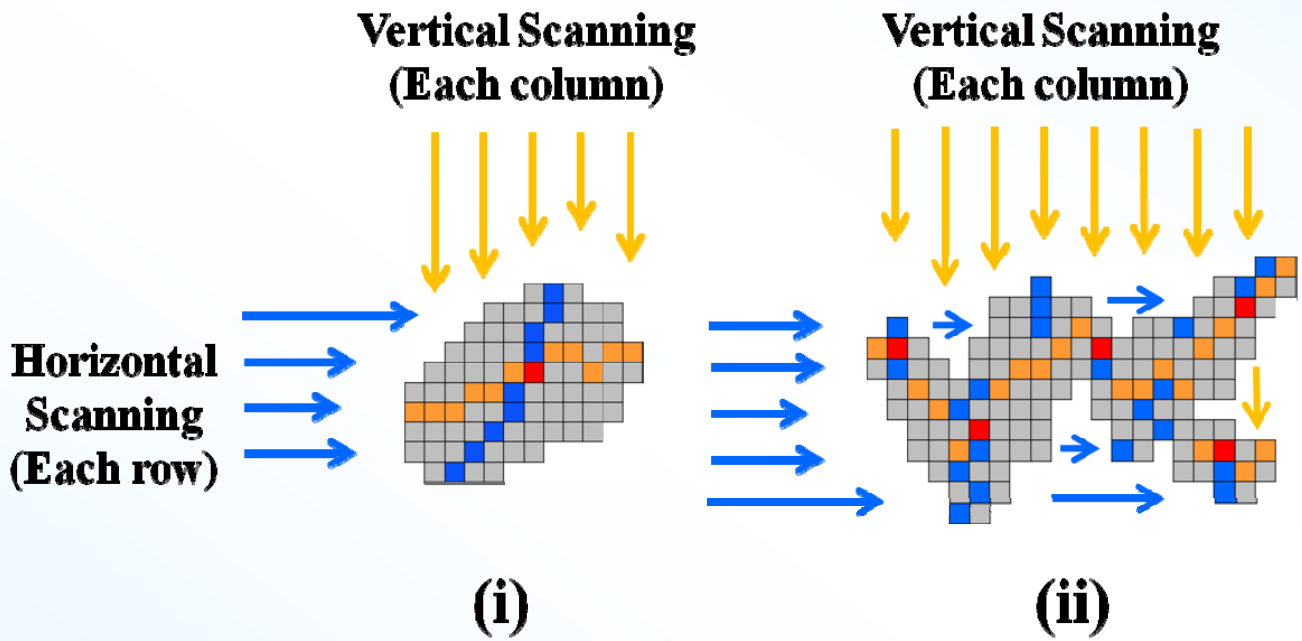

- Vertical midpoint ($m_{c,y}$)
- Midpoint pixel (m_c)
- Horizontal midpoint ($m_{c,x}$)

Nuclei Segmentation Using Distance Function Optimization

- **Goal: To estimate parameters of a single-object component**

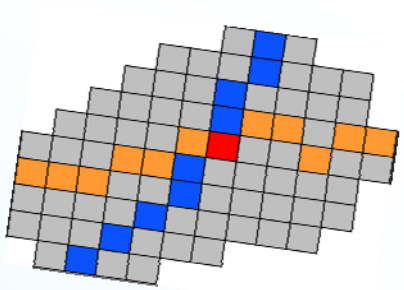

Single-object component

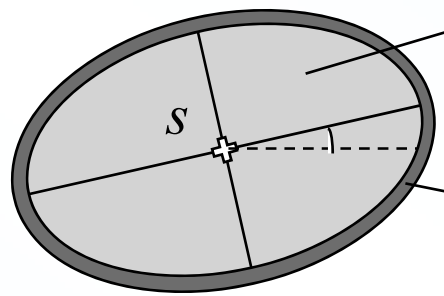

Elliptical disk $\rho = (a, b, \theta)$

(μ_1, σ_1^2)

Outer ring $(a+1, b+1, \theta)$

(μ_2, σ_2^2)

Bhattacharyya Distance *

$$B(s,\rho) = \frac{1}{4}(\mu_1(s,\rho) - \mu_2(s,\rho))^2 \sqrt{\sigma_1^2(s,\rho) + \sigma_2^2(s,\rho)}$$

$$-\frac{1}{2}\log\left(\frac{2\sigma_1(s,\rho)\sigma_2(s,\rho)}{\sigma_1^2(s,\rho) + \sigma_2^2(s,\rho)}\right)$$

Object Configuration

$$(c_\lambda, \rho_\lambda) = \arg\max_{s \in W_c, \rho \in P_\lambda} B(s,\rho)$$

* T. Kailath, "The Divergence and Bhattacharyya Distance Measures in Signal Selection," *IEEE Transactions on Communication Technology*, vol. 15, no. 1, pp. 52-60, February 1967.

Nuclei Segmentation Using Marked Point Process (MPP)

- **Goal: To estimate parameters of a multiple-object component**

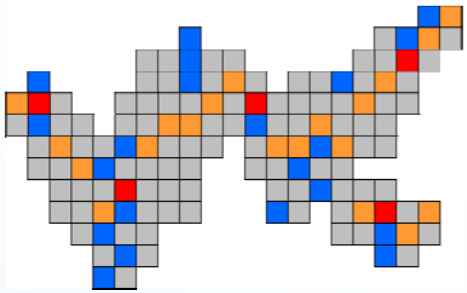

Multi-object component

We use a 2D spatial point process approach based on a stochastic birth-and-death dynamics *

We modify the energy function to include

(1) Non-uniform brightness in an image

(2) Improved object interaction

Γ **: Object configuration**

- **Our energy function**

$$H(\Gamma) = \alpha\{\sum_{(s,\rho)\in\Gamma} H_{Object}(s,\rho) + \overset{(1)}{\boxed{\sum_{s\in\Gamma_s} H_{Brightness}(s)}}\} + \sum_{s_1,s_2\in\Gamma_s} H_{Overlap}(s_1,s_2) + \overset{(2)}{\boxed{\sum_{s\in\Gamma_s} H_{Peak}(s)}}$$

*X. Descombes, R. Minlos, and E. Zhizhina. "Object extraction using a stochastic birth-and-death dynamics in continuum," *Journal of Mathematical Imaging and Vision,* Vol. 33, No. 3, pp. 347-359, March 2009.

Marked Point Process (MPP)

- **Object Energy *** $H_{Object}(s,\rho) = \begin{cases} \frac{1-B(s,\rho)}{T} & \text{if } B(s,\rho) \geq T \\ e^{\frac{B(s,\rho)-T}{3B(s,\rho)}} - 1 & \text{if } B(s,\rho) < T \end{cases}$

  - How well does an object configuration fits the image data?

- **Brightness Energy** $H_{Brightness}(s) = \tau_s$

  - Accounts for local mean brightness in the neighborhood of s

Therefore, birth energy * and birth rate *

$$H_B(s,\rho) = H_{Object}(s,\rho) + H_{Brightness}(s) \qquad b(s,\rho) = 1 + 9\frac{\max(H_B(s,\rho)) - H_B(s,\rho)}{\max(H_B(s,\rho)) - \min(H_B(s,\rho))}$$

Cumulative * $b_c(s) = \sum_{\rho \in P} b(s,\rho)$ **Normalized *** $b_n(s) = \frac{b_c(s)}{\max_{s \in \Lambda_M} b_c(s)}$

- **Overlap Energy *** $H_{Overlap}(s_1,s_2) = \max(0, 1 - \frac{\| s_1, s_2 \|}{2r})$

- **Peak Energy** $H_{Peak}(s) = \begin{cases} -h_\rho & \text{if } \sum_{\rho \in P} b_c(s) \text{ has a local maxima at} \\ 0 & \text{otherwise} \end{cases}$

Selectively Penalize Object Overlap

***X. Descombes, R. Minlos, and E. Zhizhina. "Object extraction using a stochastic birth-and-death dynamics in continuum," *Journal of Mathematical Imaging and Vision,* Vol. 33, No. 3, pp. 347-359, March 2009.**

Marked Point Process (MPP)

(I) **Determine** $H_{Object}(s,\rho)$, $H_{Brightness}(s)$, $H_B(s,\rho)$, $b(s,\rho)$, $b_c(s)$, $b_n(s)$ **and** $H_{Peak}(s)$ **for all** $s \in \Lambda_M$ **and** $\rho \in P$

(II) ***Parameter Initialization*****: Set the inverse temperature** $\beta = \beta_0$ **and the discretization step** $\delta = \delta_0$

(III) ***Configuration Initialization*****: Start with** $\Gamma = \Gamma_0$ **such that** Γ_s^0 **contains objects centered at** s **where** $b_c(s)$ **achieves local maxima and** Γ_ρ **contains their parameters** $argmax_{\rho \in P} b(s,\rho)$ **for each** s **respectively**

(IV) ***Birth Step*****: For each** $s \in \Lambda_M$**, if** $s \notin \Gamma_s$ **add a point at** s **with probability** $\delta b_n(s)$ **and give birth to an object of** ρ **with probability** $\frac{b(s,\rho)}{\sum_{\rho \in P} b(s,\rho)}$

(V) ***Death Step*****: Sort the configuration of points** Γ **in descending order of** $H_B(s,\rho)$**. For each sorted point** s **obtain death rate** $d(s,\rho) = \frac{\delta a(s)}{1+\delta a(s)}$**, where** $a(s) = e^{-\beta(H(\Gamma/\{s,\rho\}) - H(\Gamma))}$ **and kill the object with probability** $d(s)$

(VI) Convergence Test: If all the objects born in the *Birth Step* are killed in the *Death Step*, stop. Otherwise, increase β **and decrease** δ **by geometric scheme using common ratios** Δ_β **and** Δ_δ **and go back to the *Birth Step***

X. Descombes, R. Minlos, E. Zhizhina,"Object extraction using a stochastic birth-and-death dynamics in continuum," *Journal of Mathematical Imaging and Vision,* Vol. 33, No. 3, pp. 347-359, March 2009.

Segmentation Results

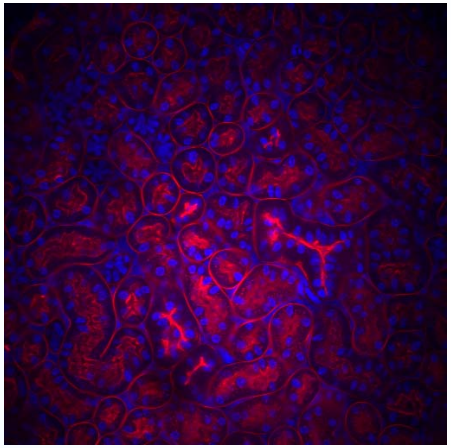

Original Three Channel Image

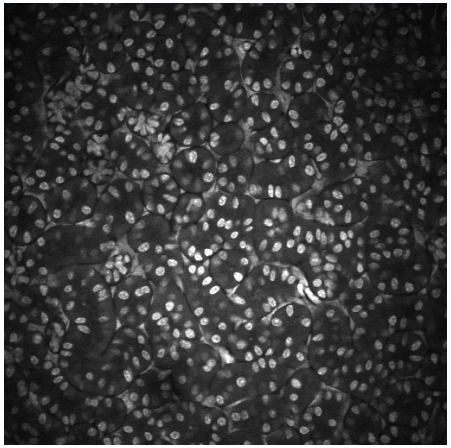

Blue Channel

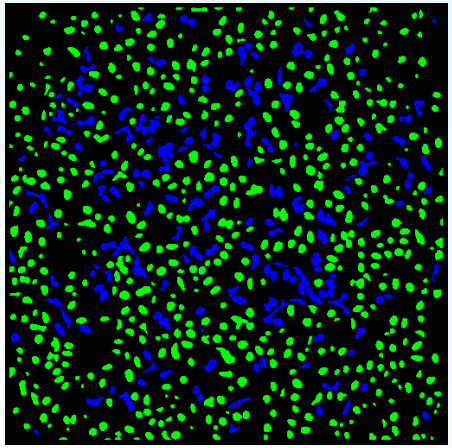

Classified Components

N = 628

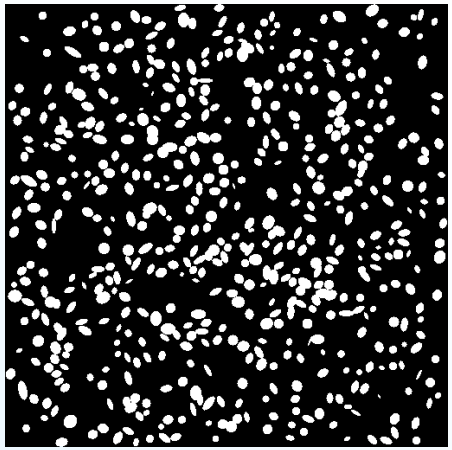

Segmentation Results

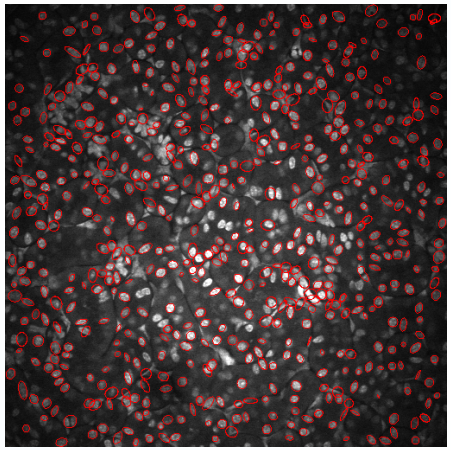

Segmentation Results (Overlaid)

Experimental Results: Comparison

MPP Method from [Ref]

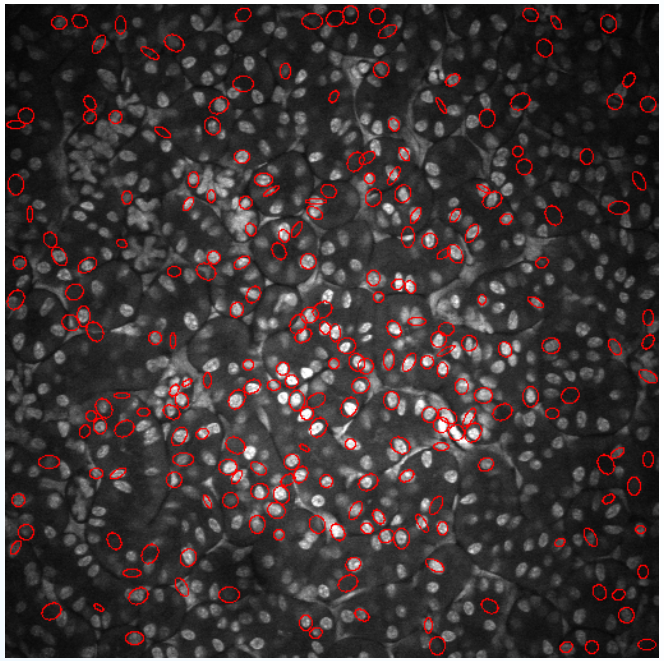

N = 241

Our Proposed Method

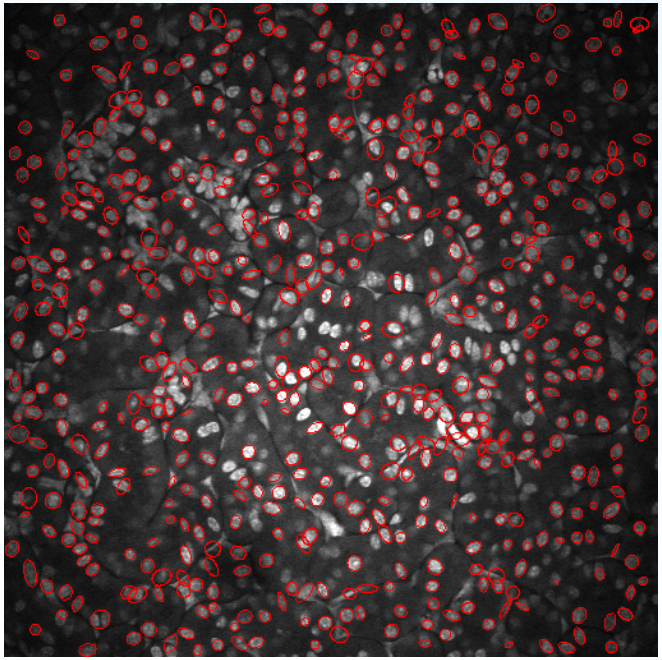

N = 628

Average Processing Time:
20 times faster

[Ref] X. Descombes, R. Minlos, E. Zhizhina,"Object extraction using a stochastic birth-and-death dynamics in continuum," *Journal of Mathematical Imaging and Vision,* Vol. 33, No. 3, pp. 347-359, March 2009.

3D Active Contours with Inhomogeneity Correction (3DacIC)

Introduction

- **We propose a method (3DacIC) that segments 3D microscopy volumes based upon a combination of**
  - **3D region-based active contours**
  - **3D inhomogeneity correction**

Energy Function of 3Dac

- **3Dac: Extension version of 2Dac such that**

$$E = \lambda_1 \int_{in(\phi_{z_p})} \left| I^O_{z_p}(\mathbf{x}) - c_1 \right|^2 d\mathbf{x} + \lambda_2 \int_{out(\phi_{z_p})} \left| I^O_{z_p}(\mathbf{x}) - c_2 \right|^2 d\mathbf{x}$$

$$+ \mu \cdot Surface(\phi_{z_p}(\mathbf{x})) \quad \text{where } \mathbf{x} \in \Re^3$$

  - **$I^O_{z_p}$(x): the pth image in a volume to be analyzed where $p \in \{1, 2, \ldots, P\}$**
  - **ϕ_{z_p}(x): zero-level curve (Lipschitz function)**
  - **c_1, c_2 : Mean intensities inside of ϕ_{z_p} and outside of ϕ_{z_p}**
    - **Note that c_1 and c_2 are vectors with three elements (3 × 1 vectors)**
  - **λ_1, λ_2, μ: Weight coefficients for each term**

Proposed Energy Function (3DacIC)

- **Utilizing Heaviside's function, $H(\cdot)$, the Dirac delta function, $\delta(\cdot)$ and swapping order of the integrals yields**

$$E = \lambda_1 \int_\Omega \left((I^O)^2 \circ 1_K - 2I^O \circ (W * K)c_1 + (W^2 * K)c_1^2 \right) H(\phi) d\mathbf{x}$$
$$+ \lambda_2 \int_\Omega \left((I^O)^2 \circ 1_K - 2I^O \circ (W * K)c_2 + (W^2 * K)c_2^2 \right) (1 - H(\phi)) d\mathbf{x}$$
$$+ \mu \int_\Omega \delta(\phi) \left| \nabla \phi \right| d\mathbf{x}$$

  - **where * is 3D convolution operation and $1_K(\mathbf{x})$ is a 3D volume of same size as $I^O_{z_p}(\mathbf{x})$ whose entries are all 1 except near the volume boundary Ω**
  - **Note that $1_K(\mathbf{x})$ is obtained by convolving a 3D matrix of ones with 3D kernel K.**
  - **For brevity we have omitted the subscript z_p and the explicit argument x**

Segmentation Results and Inhomogeneity Corrected Images at Various Depth for WSM Images

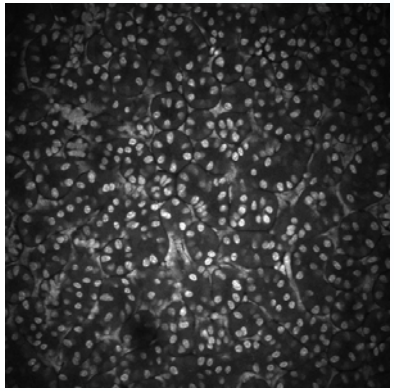

Original 100th image

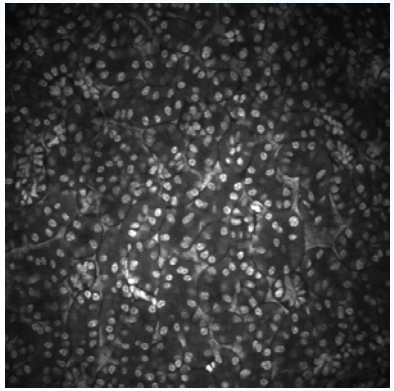

Original 200th image

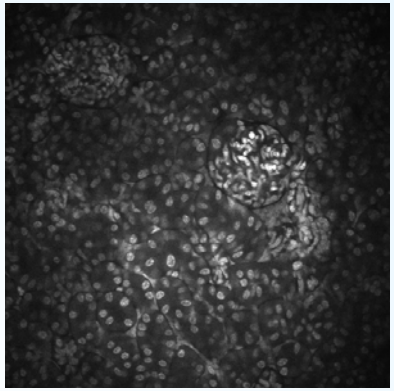

Original 300th image

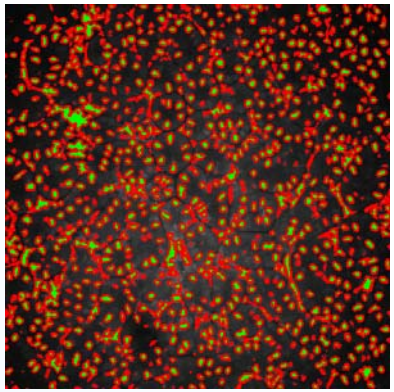

3DacIC (Proposed)

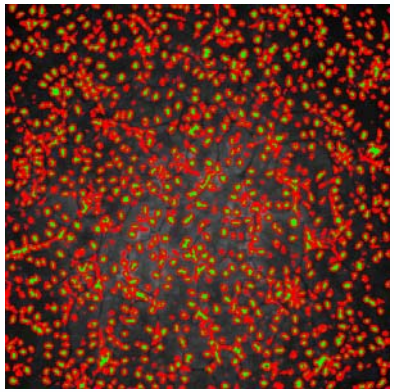

3DacIC (Proposed)

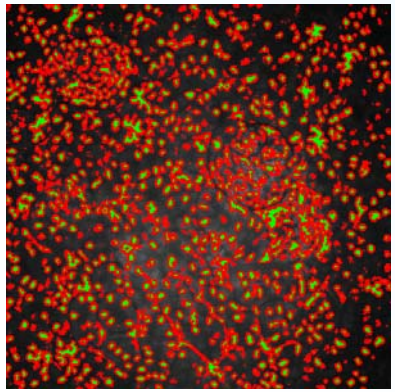

3DacIC (Proposed)

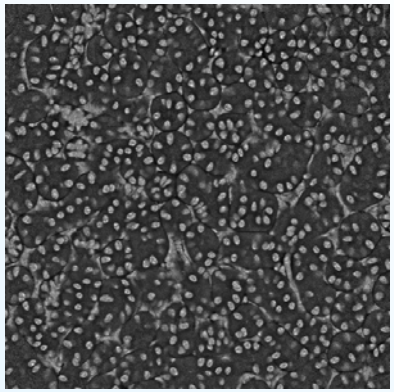

Inhomogeneity corrected

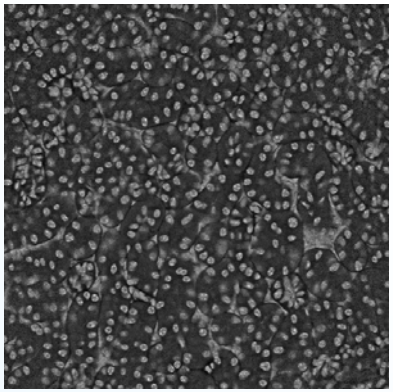

Inhomogeneity corrected

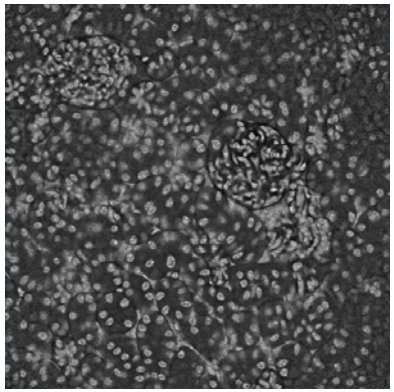

Inhomogeneity corrected

Results Comparison – Flipped Nuclei Stack A 7th Images (Red: Nuclei Contours, Green: Nuclei Regions)

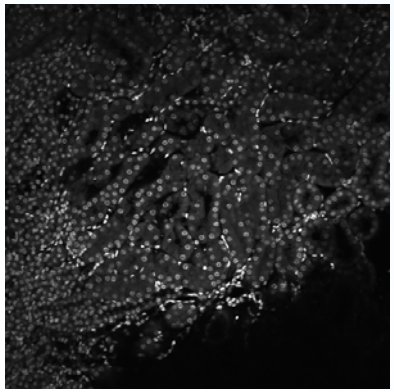

Original

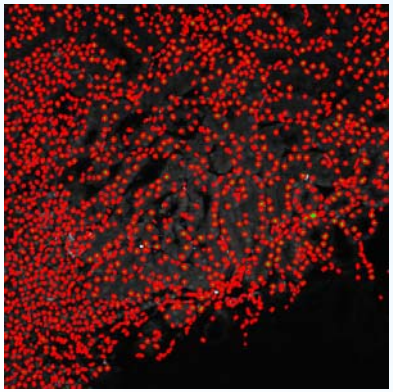

Ground truth

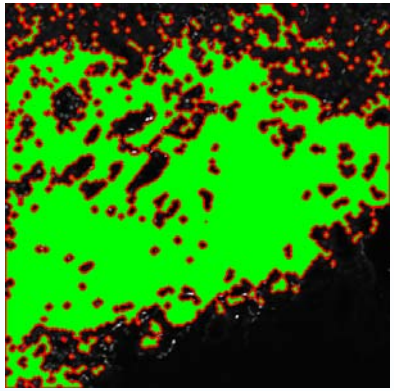

2Dac [1]

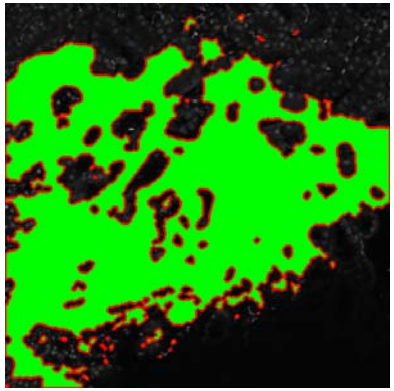

2Dlac [2]

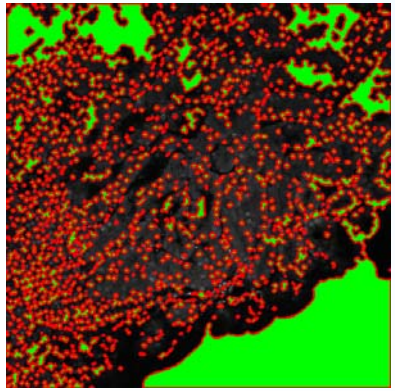

2DacIC [3]

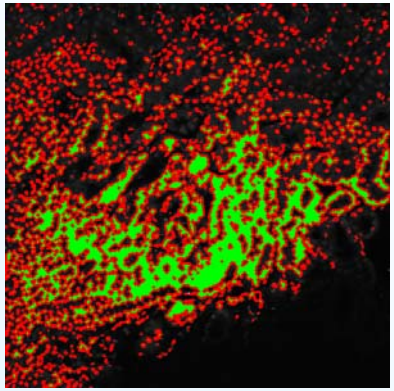

3Dac [4, 5]

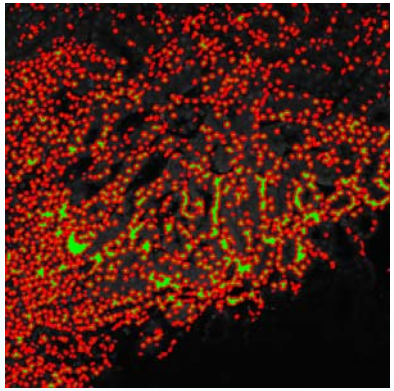

3Dsquassh [6]

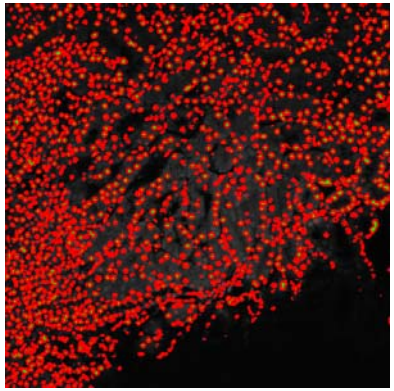

3DacIC (Proposed)

Results Comparison – Flipped Nuclei Stack B 16th Images (Red: Nuclei Contours, Green: Nuclei Regions)

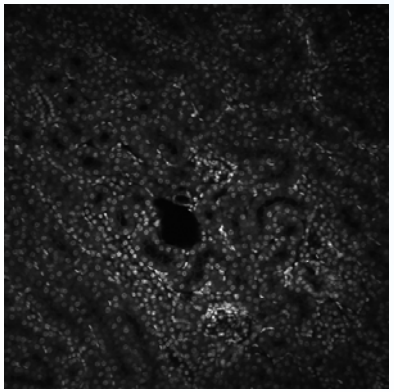

Original

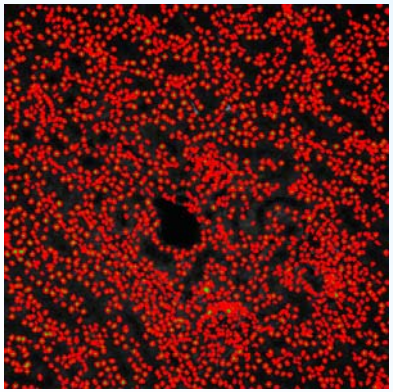

Ground truth

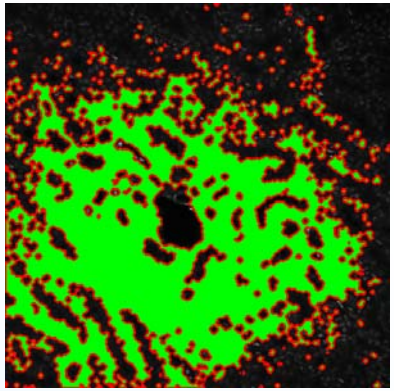

2Dac [1]

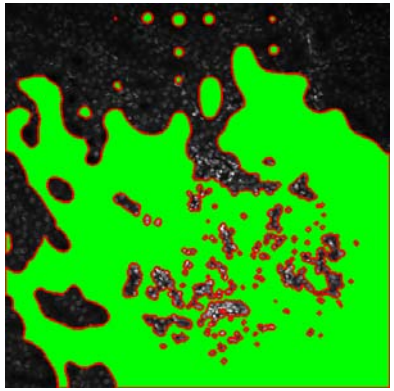

2Dlac [2]

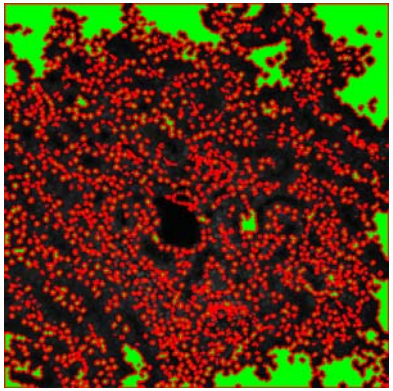

2DacIC [3]

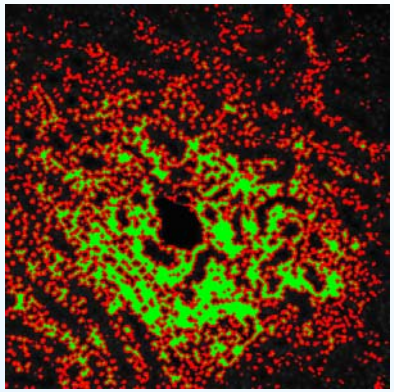

3Dac [4, 5]

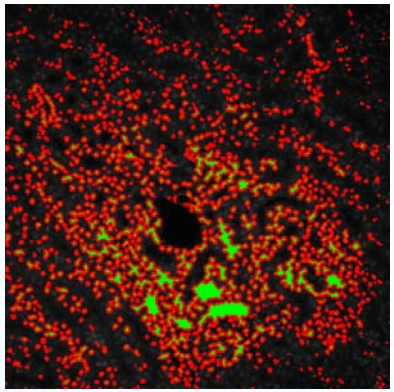

3Dsquassh [6]

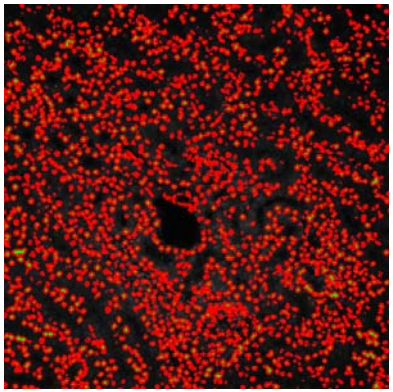

3DacIC (Proposed)

Accuracy - Type I and Type II Errors

- ***TP*: Nuclei pixels correctly detected as nuclei pixels in segmented image**
- ***TN*: Background correctly detected as background in segmented image**
- ***FP*: Background wrongly detected as nuclei pixels in segmented image**
- ***FN*: Nuclei pixels wrongly detected as background in segmented image**
- ***Tot*: Total number of image pixels**

$$Accuracy = \frac{TP + TN}{Tot}, \quad TypeI = \frac{FP}{Tot}, \quad TypeII = \frac{FN}{Tot}$$

Flipped Nuclei Stack A Blue 7th Image

	Accuracy	Type I	Type II
2Dac	54.7066%	43.3144%	1.9791%
2Dlac	57.6168%	39.1350%	3.2482%
2DacIC	73.1171%	25.0900%	**1.7929%**
3Dac	79.7585%	16.6313%	3.6102%
3Dsquassh	88.7196%	8.5674%	2.7130%
3DacIC (Proposed)	**91.8678%**	**5.6053%**	2.5269%

- **Type-I error (False Alarm): False detection**
- **Type-II error (Missed): Missing detection**

Flipped Nuclei Stack B Blue 16th Image

	Accuracy	Type I	Type II
2Dac	61.8896%	32.4192%	5.6911%
2Dlac	58.2088%	31.5224%	10.2688%
2DacIC	80.3520%	15.1890%	**4.4590%**
3Dac	78.4348%	15.1447%	6.4205%
3Dsquassh	85.3157%	5.9555%	8.7288%
3DacIC (Proposed)	**89.6511%**	**4.4998%**	5.8491%

- **Type-I error (False Alarm): False detection**
- **Type-II error (Missed): Missing detection**

Flipped Nuclei Stack A1 Blue 18th Image

	Accuracy	Type I	Type II
2Dac	57.3856%	38.9107%	3.7037%
2Dlac	66.3521%	28.1330%	5.5149%
2DacIC	86.1752%	11.3010%	2.5238%
3Dac	72.8584%	24.9794%	**2.1622%**
3Dsquassh	83.3508%	14.2776%	2.3716%
3DacIC (Proposed)	**87.7125%**	**9.4864%**	2.8011%

- **Type-I error (False Alarm): False detection**
- **Type-II error (Missed): Missing detection**

Flipped Nuclei Stack B1 Blue 18th Image

	Accuracy	Type I	Type II
2Dac	72.2759%	20.4388%	7.2853%
2Dlac	63.4697%	27.4529%	9.0775%
2DacIC	87.6350%	8.9874%	**3.3775%**
3Dac	81.5754%	12.5660%	5.8586%
3Dsquassh	83.2233%	13.0070%	3.7697%
3DacIC (Proposed)	**89.0999%**	**7.0015%**	3.8986%

- **Type-I error (False Alarm): False detection**
- **Type-II error (Missed): Missing detection**

3D Segmentation Results of Each Dataset (Green: Nuclei Regions)

- **3D visualization using Voxx**
- **Each dataset (WSM, Flipped Nuclei Stack A, and Flipped Nuclei Stack B) was cropped into subvolumes $60 \times 60 \times 20$, respectively**

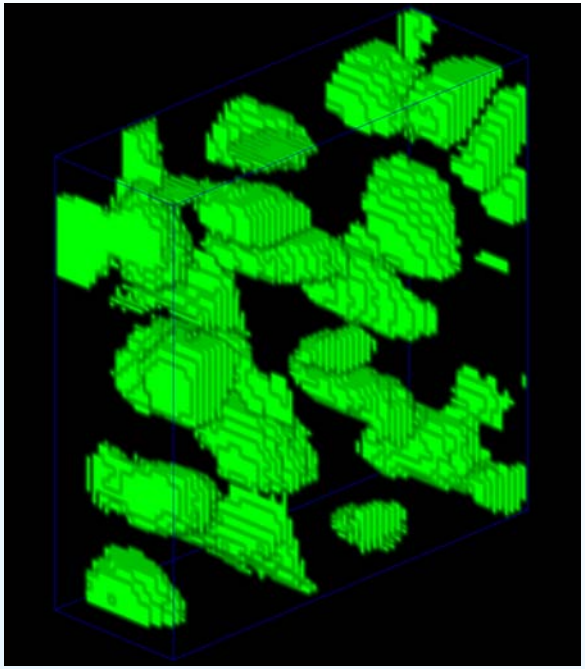

WSM

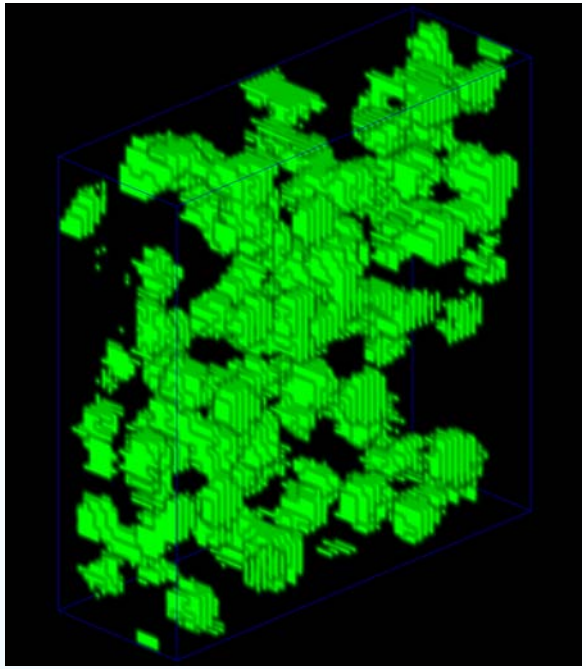

Flipped Nuclei Stack A

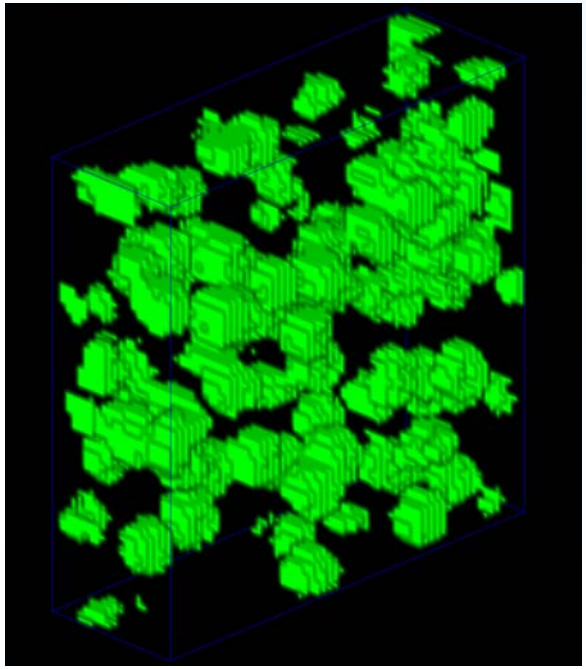

Flipped Nuclei Stack B

$2D^+$ Convolutional Neural Networks (CNN)

Research Goal

- **25x-water-scale-mount (*wsm*) from rat kidney using two-photon microscopy**
  - **X = 512, Y = 512, P = 512, Q = 1, R = 1**
- **Fluorescent molecules label nuclei**
- **The goal is to segment the nuclei**

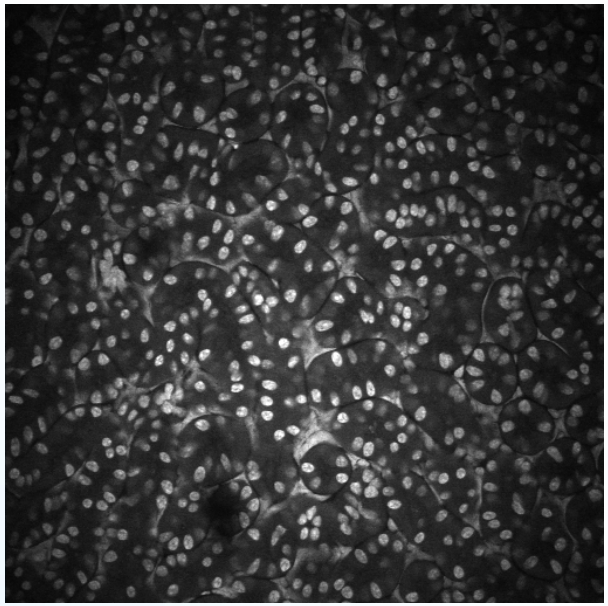

wsm $\mathbf{I}_{z_{70}}$

Proposed Method

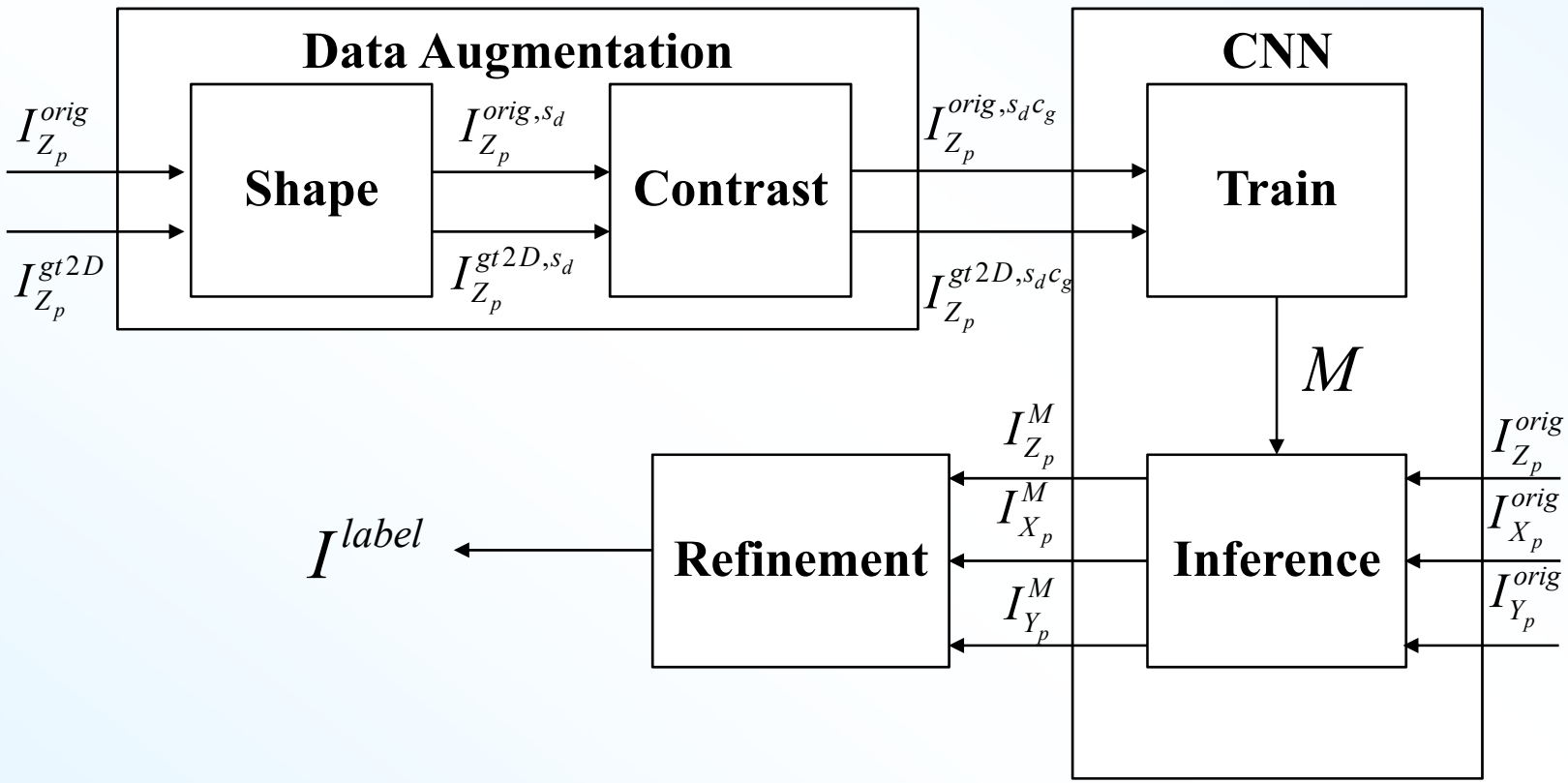

Data Augmentation

- Water-scale-mount blue channel (512 images)
  - We have 11 groundtruth images
  - 10 images are used for data augmentation
- Elastic Deformation (faked shape)
- Gamma Correction (faked contrast)
- For each ground truth image:
  - First generated 100 images with faked shape
  - Second generated 10 more images with faked contrast on each faked shape image
  - Total 1000 augmented images are generated

Data Augmentation

- **Elastic deformation:**
  - **A grid of control points with 64 pixel spacing in the x and y directions is created for each input image**
  - **Control points are then randomly displaced in both the x and y directions to within ±15 pixels**
  - **B-spline is fit to the grid of displaced control points**
  - **Bicubic interpolation to warp each pixel to its new coordinates**
  - **Ground truth images are transformed accordingly**
- **Gamma Correction**
  - $v = 255\left(\frac{u}{255}\right)^{\frac{1}{\gamma}}$, $\gamma = \frac{\log(\frac{1}{2})}{\log(\frac{g}{255})}$
  - $g \in \{80, 90, \ldots, 160\}$

Example

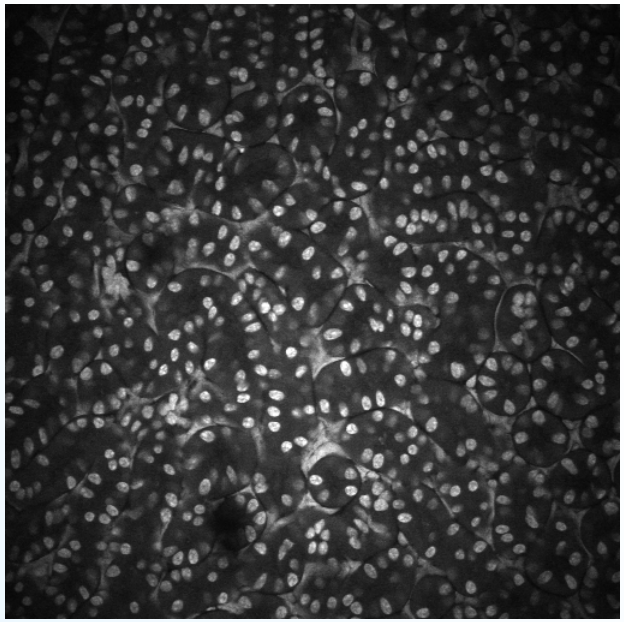

Water-scale-mount blue 70th original image

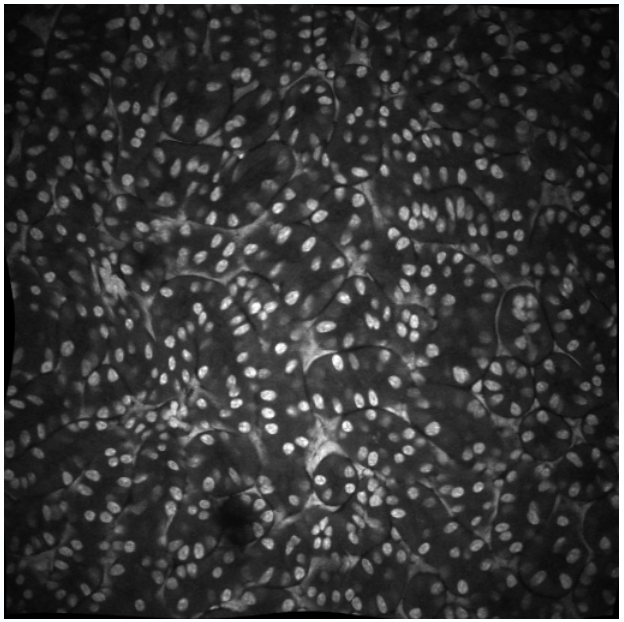

Elastic Deformation

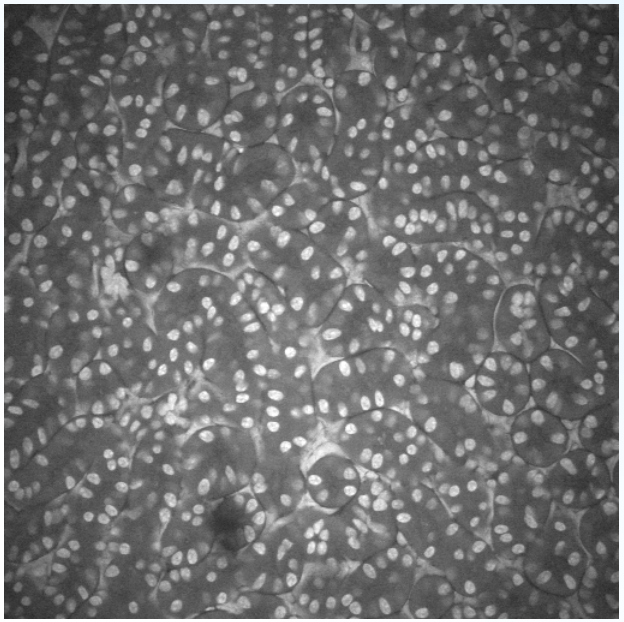

Gamma Correction

Data-I

CNN Architecture

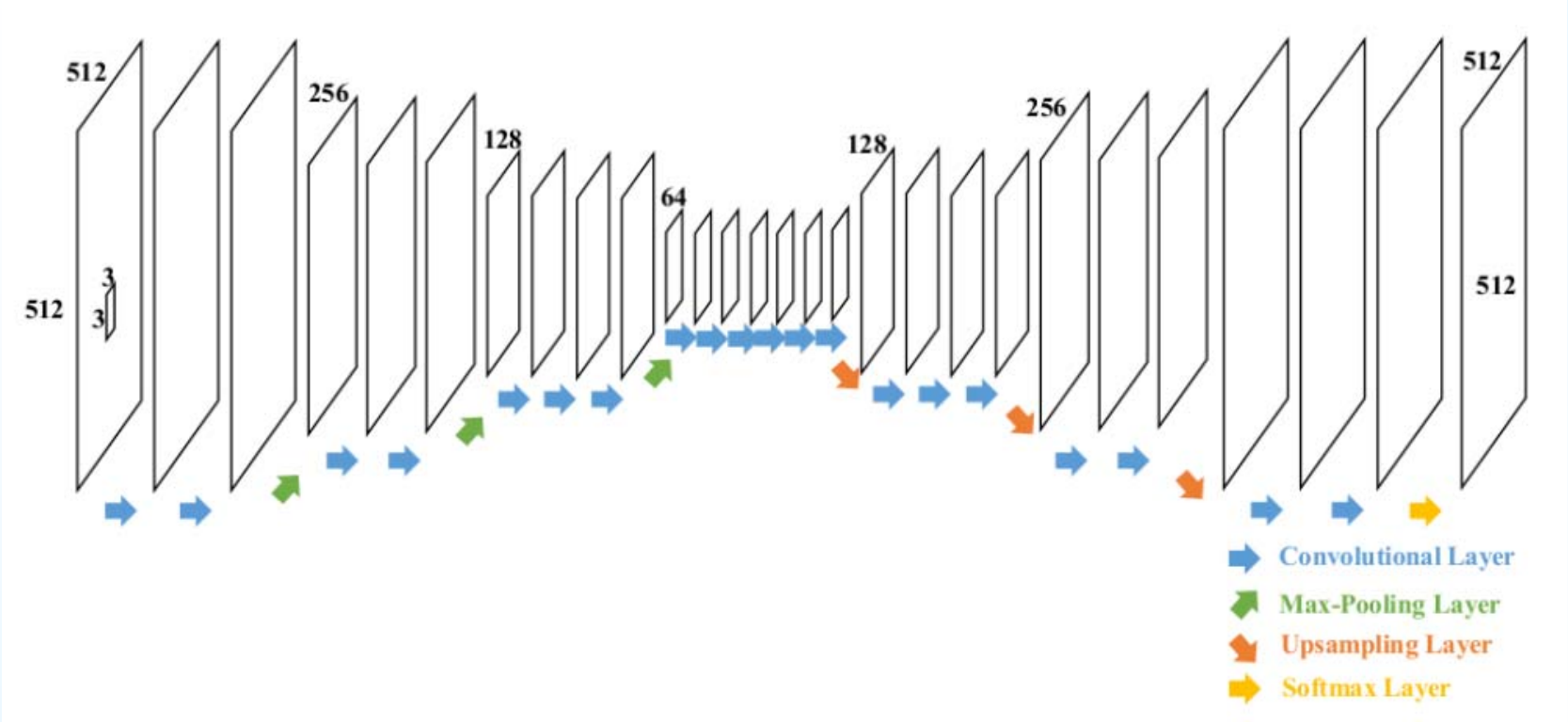

Architecture of our convolutional neural network

3D Groundtruth

- **Hand-segmented nuclei in a volume of 32x32x32 by labeling each images**

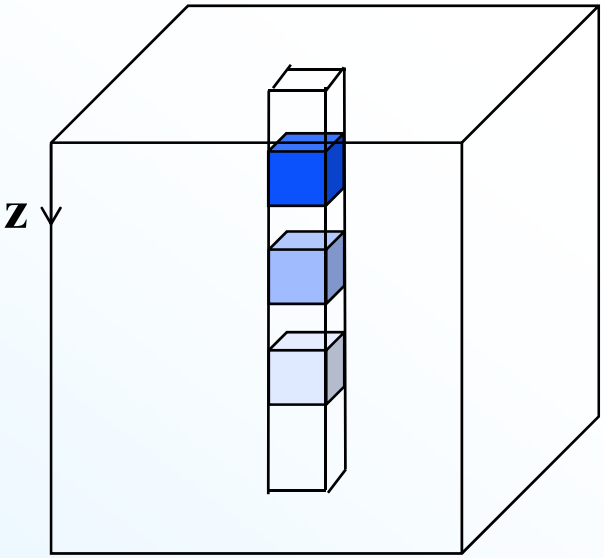

Water-scale-mount blue

Volume1	$241 \le x \le 272$	$241 \le y \le 272$	$31 \le z \le 62$
Volume2	$241 \le x \le 272$	$241 \le y \le 272$	$131 \le z \le 162$
Volume3	$241 \le x \le 272$	$241 \le y \le 272$	$231 \le z \le 262$

Results

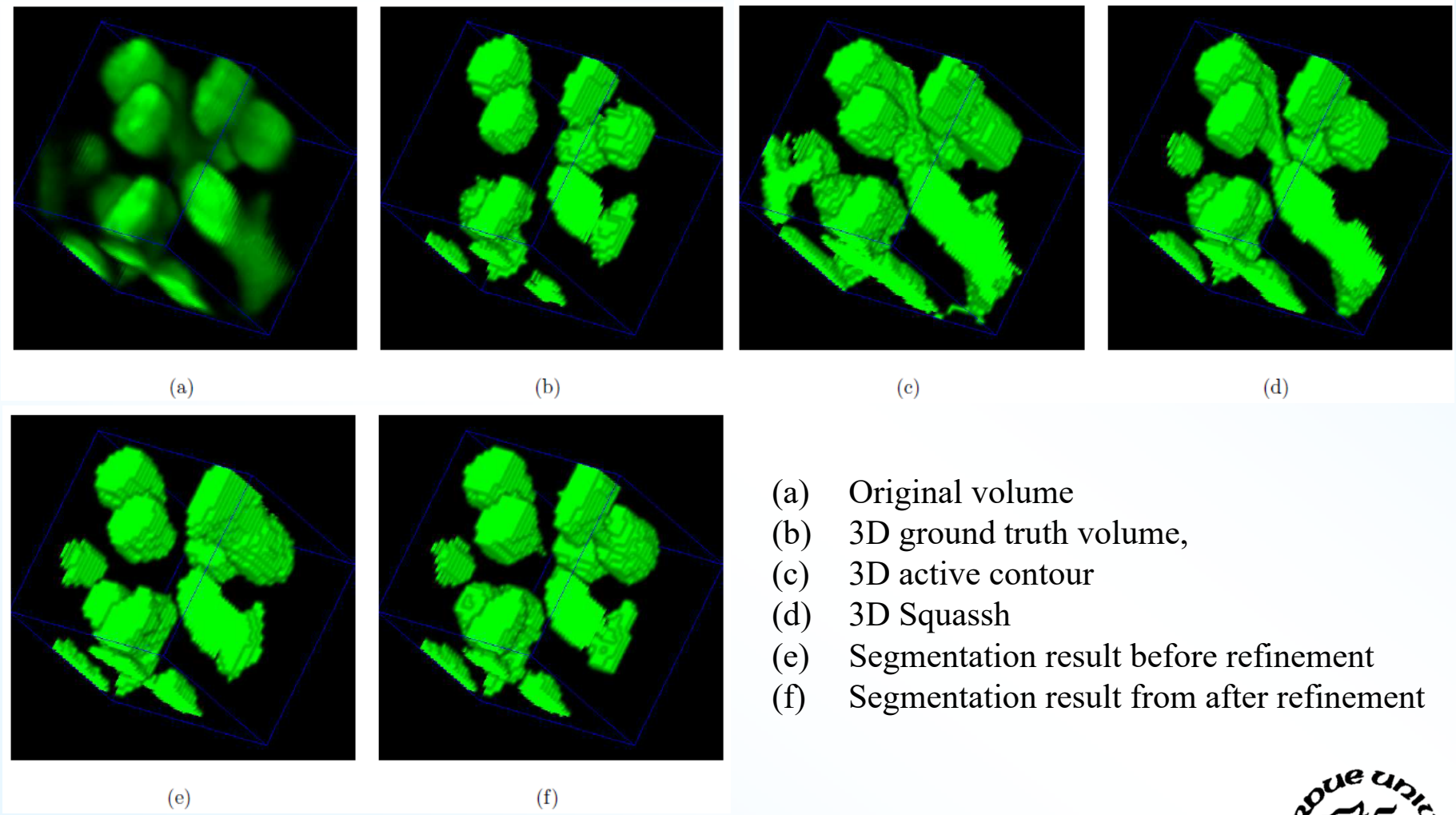

(a) Original volume
(b) 3D ground truth volume,
(c) 3D active contour
(d) 3D Squassh
(e) Segmentation result before refinement
(f) Segmentation result from after refinement

Results

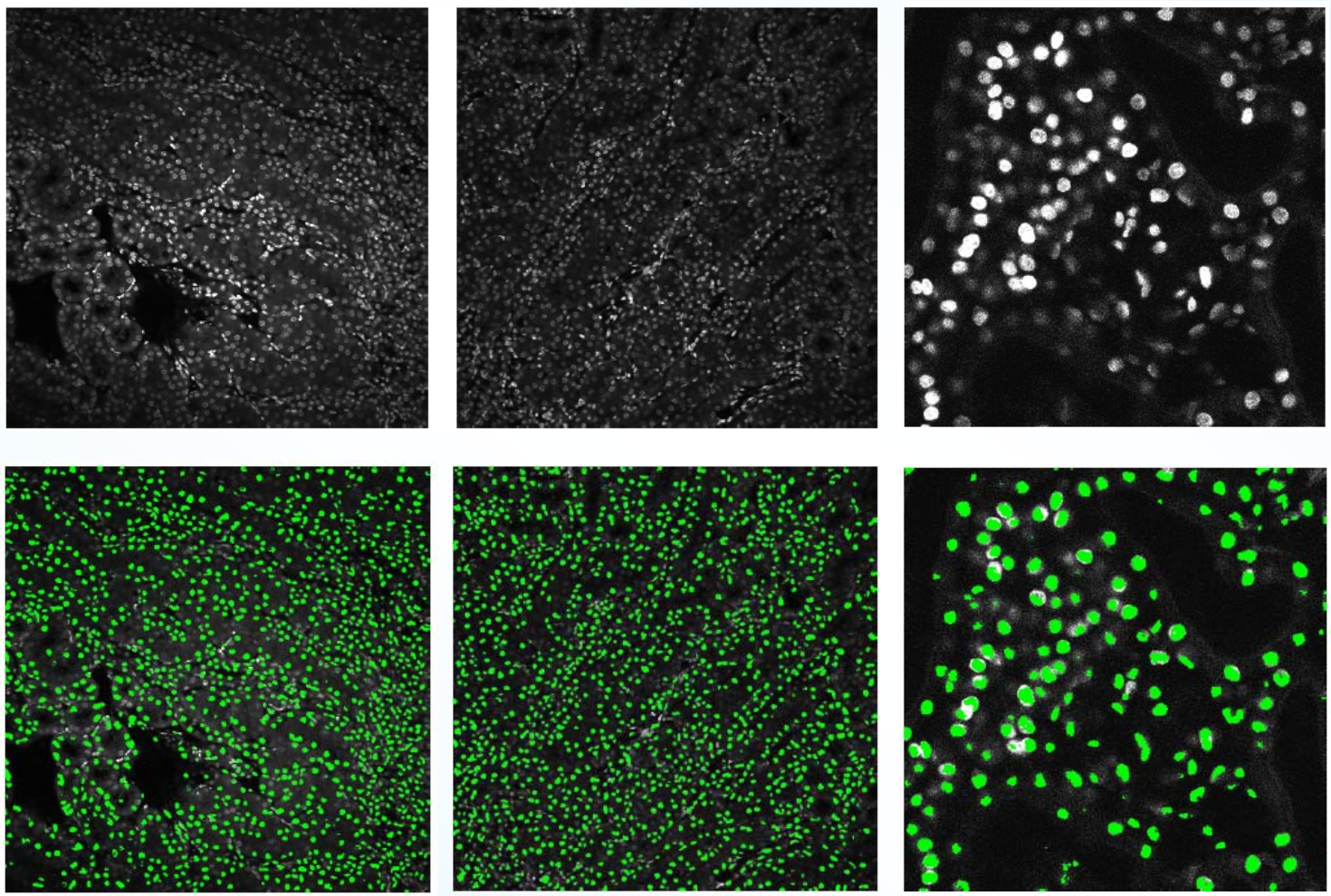

Data-II **Data-III** **Data-IV**

Accuracy

		3D Active Contour	Squassh	Our Method
Volume I	Accuracy	84.62%	90.14%	94.25%
	Type-I	14.80%	9.07%	5.18%
	Type-II	0.25%	0.79%	0.57%
Volume II	Accuracy	79.67%	88.26%	95.24%
	Type-I	20.16%	11.67%	4.18%
	Type-II	0.16%	0.07%	0.58%
Volume II	Accuracy	76.72%	87.29%	93.21%
	Type-I	23.24%	12.61%	6.61%
	Type-II	0.05%	0.10%	0.18%

- **Type-I error (False Alarm): False detection**
- **Type-II error (Missed): Missing detection**

3D Convolutional Neural Networks (CNN)

Block Diagram

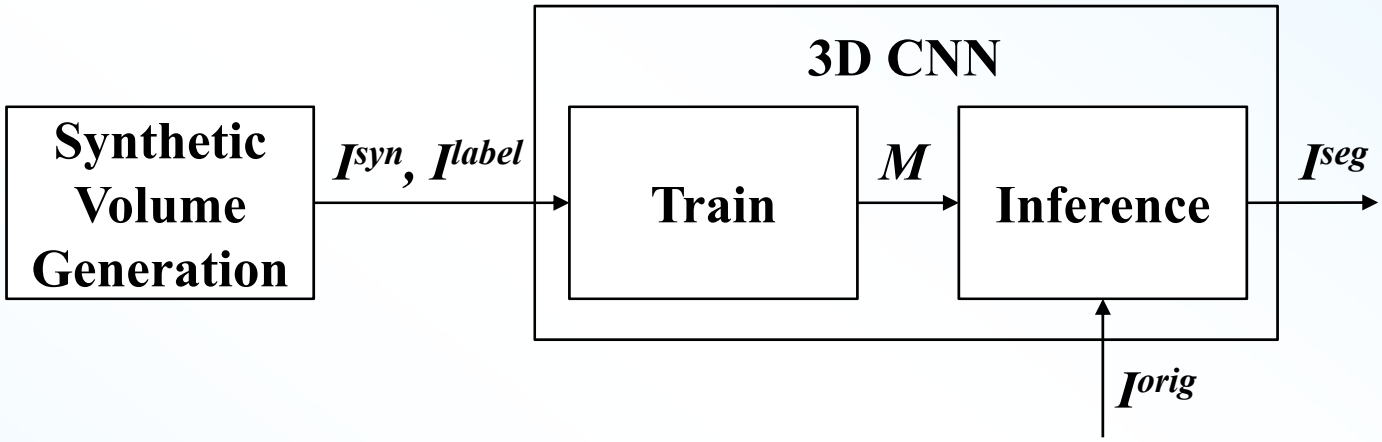

I^{syn}: 3D synthetic image volume
I^{label}: 3D labeled image volume of I^{syn}
I^{orig}: 3D real image volume
I^{seg}: 3D segmented image volume
M: trained 3D CNN model

Synthetic Volume Generation

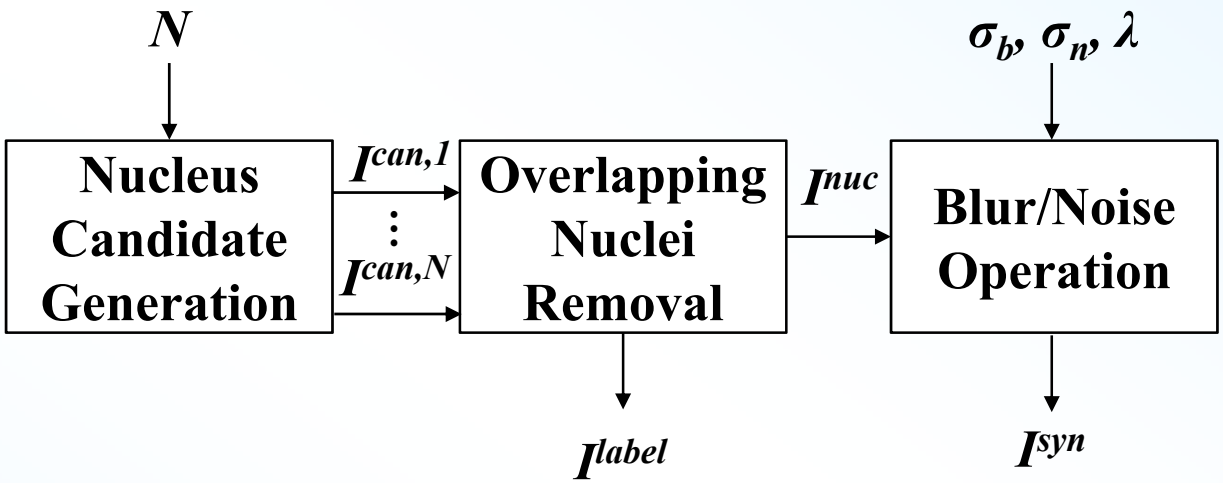

N: the number of nuclei candidates
$I^{can,j}$: the j-th nucleus candidate
I^{nuc}: a volume with multiple nuclei
σ_b: standard deviation of blur operation
σ_n: standard deviation of Gaussian noise
λ: mean of Poisson noise

Synthetic Volumes Examples

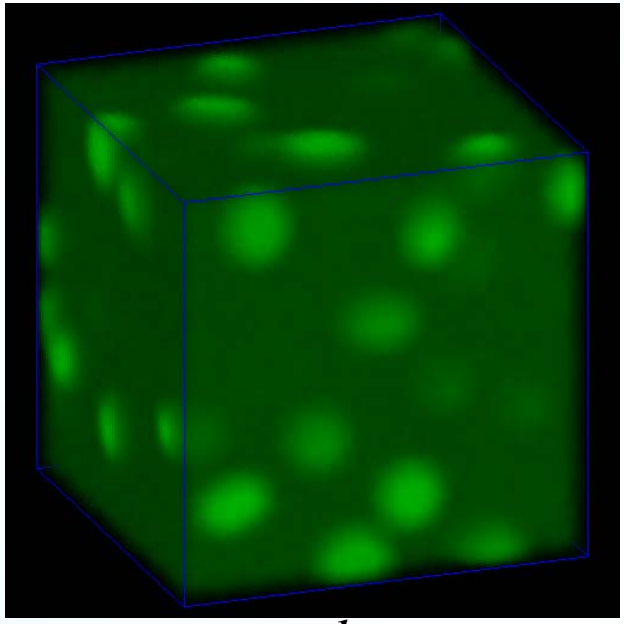

$I^{syn,1}$

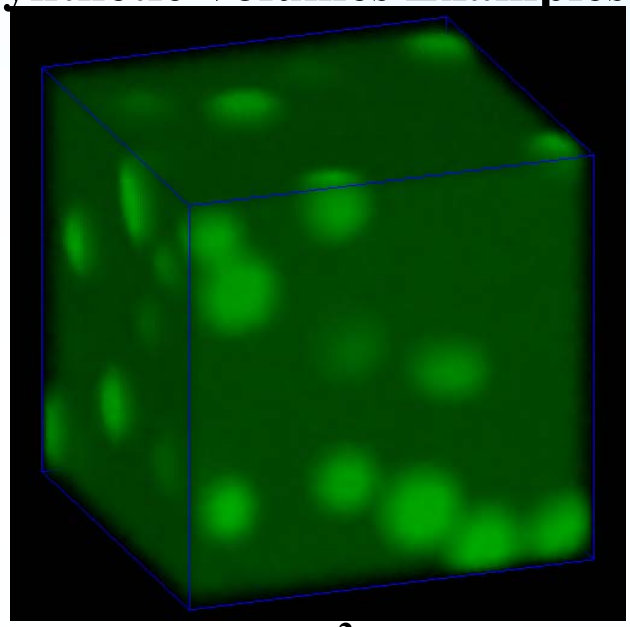

$I^{syn,2}$

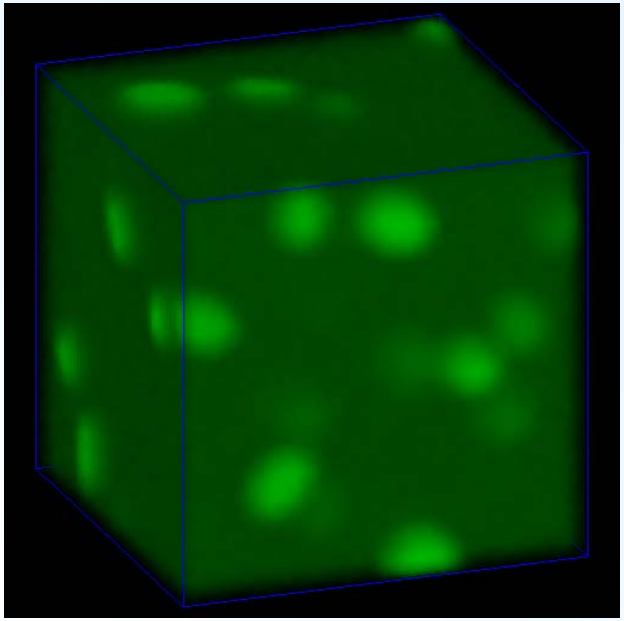

$I^{syn,3}$

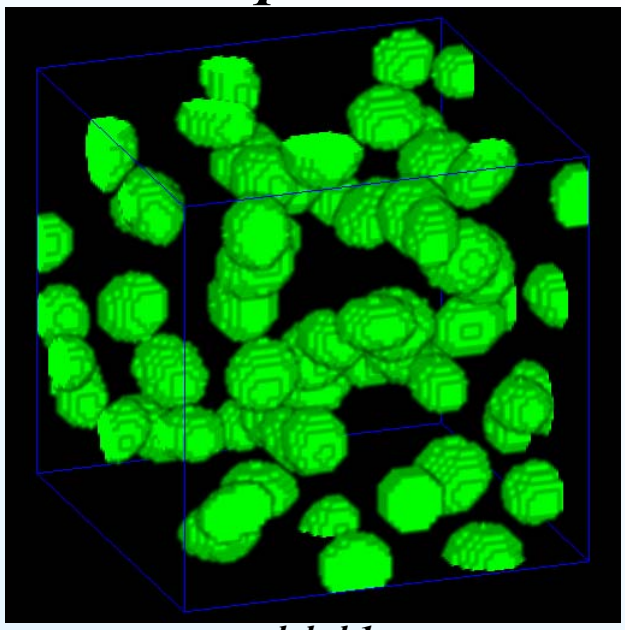

$I^{label,1}$

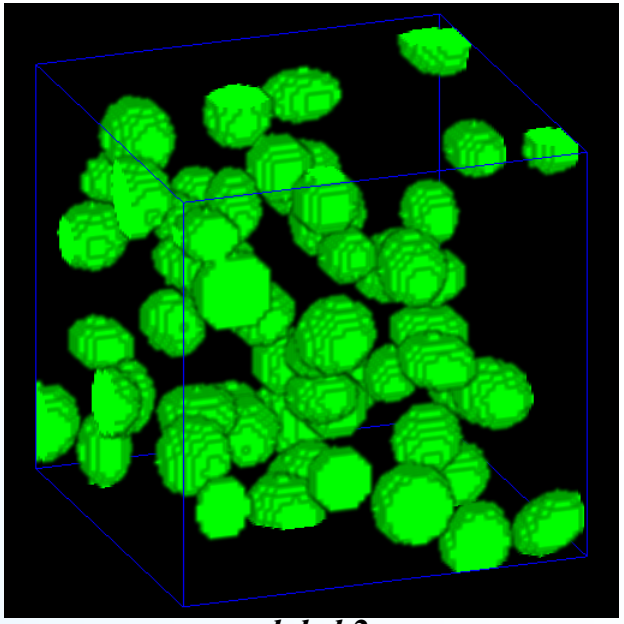

$I^{label,2}$

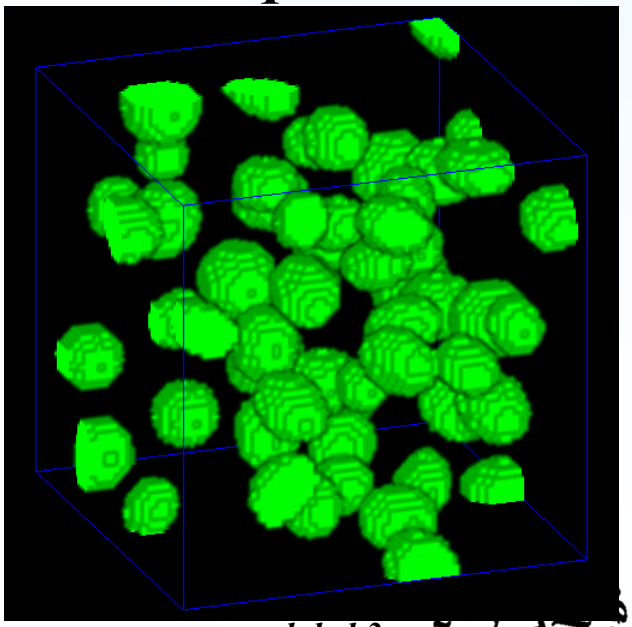

$I^{label,3}$

3D CNN Architecture

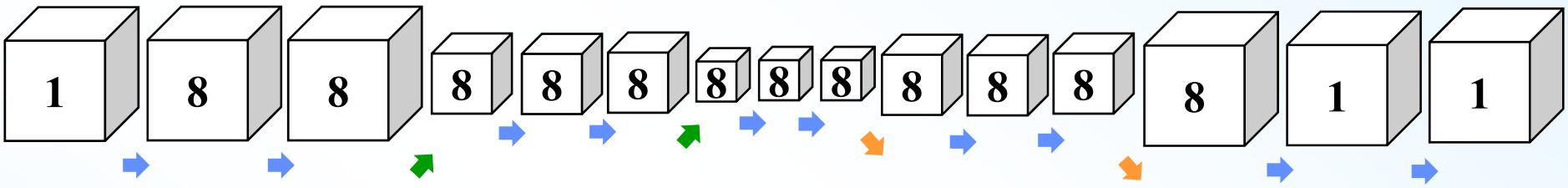

3D Convolutional Layer
3D Max-Pooling Layer
3D Max-Unpooling Layer

- The size of the input volume is 64 × 64 × 64
- 3D Convolutional Layer
  - The kernel size is 5 × 5 × 3
  - 3D Batch Normalization
  - Activation Function: ReLU
- 3D Max-Pooling Layer/3D Max-Unpooling Layer
  - The downsampling/upsampling rate in each dimension is 2
  - The stride in each dimension is 2
- The size of the output volume is 64 × 64 × 64
- 100 training volumes are used
- 17000 iterations

Result

		3Dac	3DacIC	3D Squassh	$2D^+$ CNN	3D CNN
Volume1	**Acc.**	**84.09%**	**87.36**	**90.14%**	**94.25%**	**92.20%**
	Type-1	15.68%	12.44	90.7%	5.18%	5.38%
	Type-2	0.23%	0.20	0.79%	0.57%	2.42%
Volume2	**Acc.**	**79.25%**	**86.78**	**88.26%**	**95.24%**	**92.32%**
	Type-1	20.71%	13.12	11.67%	4.18%	6.81%
	Type-2	0.04%	0.10	0.07%	0.58%	0.87%
Volume3	**Acc.**	**76.44%**	**83.47**	**87.29%**	**93.21%**	**94.26%**
	Type-1	23.55%	16.53	12.61%	6.61%	5.19%
	Type-2	0.01%	0.00	0.10%	0.18%	0.55%

$$\text{Accuracy} = \frac{n_{\text{TP}} + n_{\text{TN}}}{n_{\text{total}}} \qquad \text{Type-I Error} = \frac{n_{\text{FP}}}{n_{\text{total}}} \qquad \text{Type-II Error} = \frac{n_{\text{FN}}}{n_{\text{total}}}$$

False-Positive: The output image classifies as nuclei where the groundtruth image classifies as background

False-Negative: The output image classifies as background where the groundtruth image classifies as nuclei

Volume 1 Result

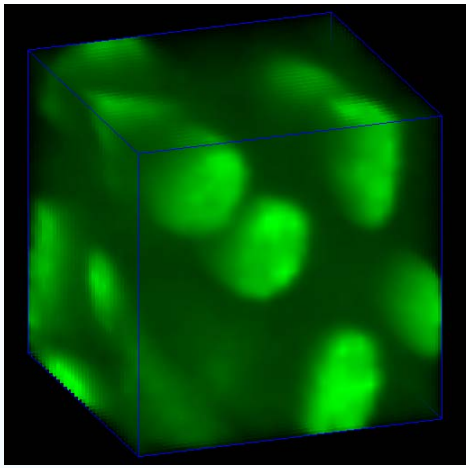

Original

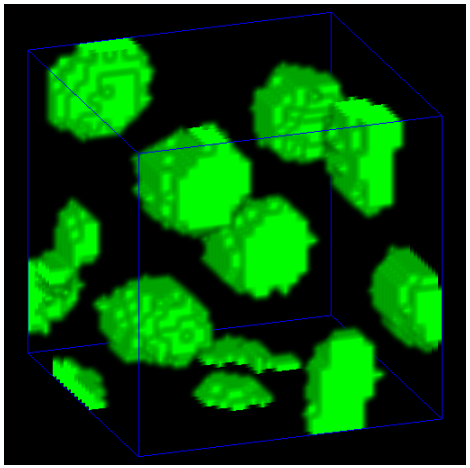

3D ground truth

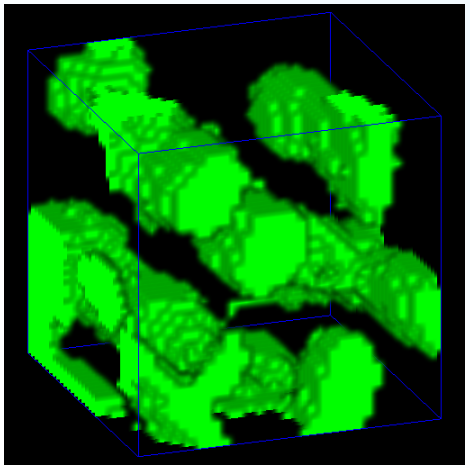

3Dac

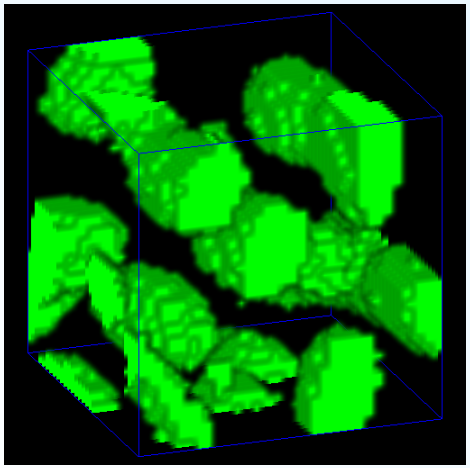

3DacIC

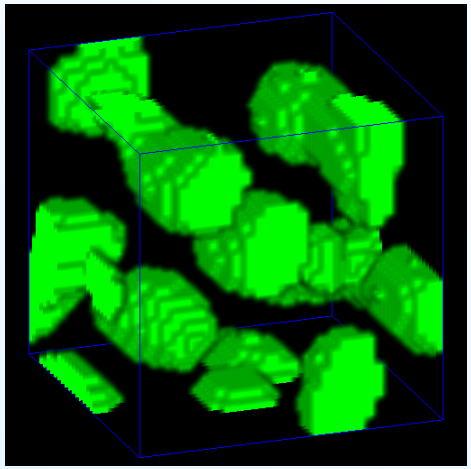

3D Squassh

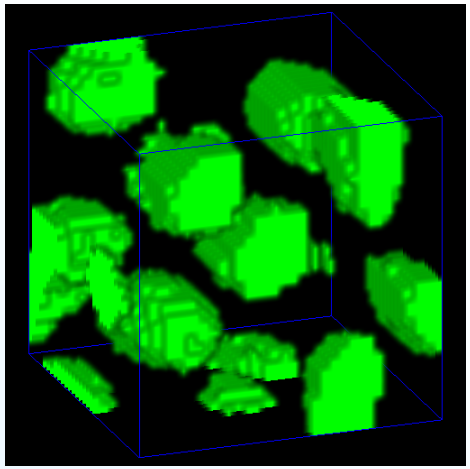

$2D^{+}$ CNN

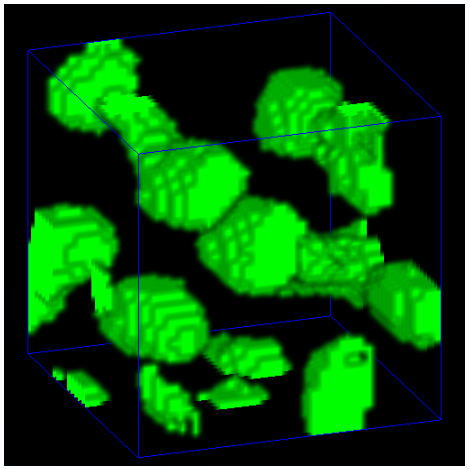

3D CNN

Volume 2 Result

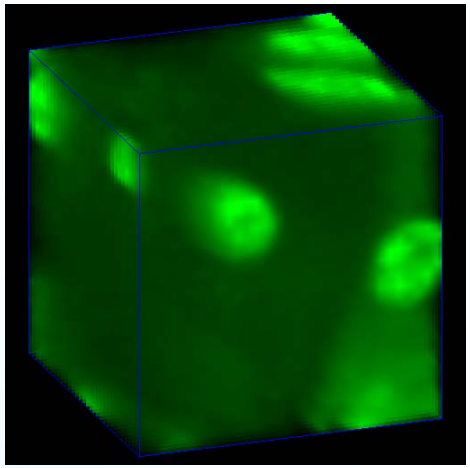

Original

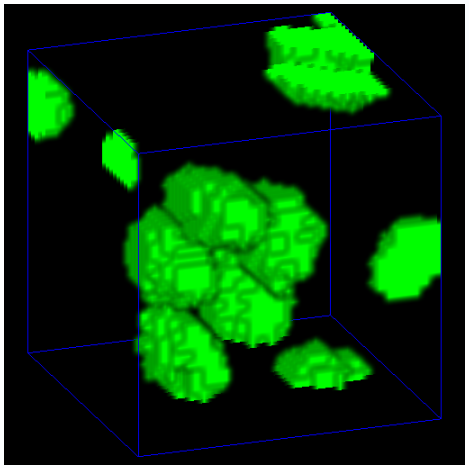

3D ground truth

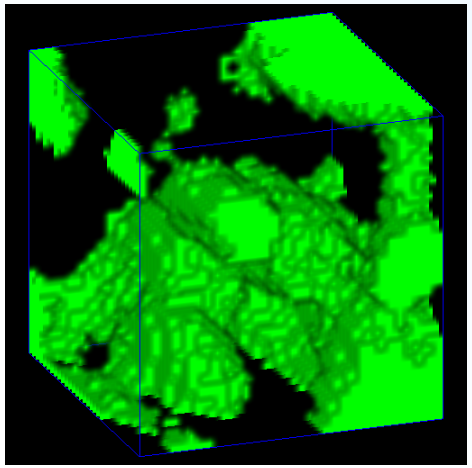

3Dac

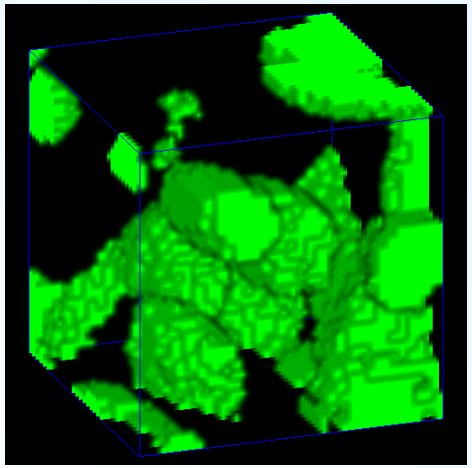

3DacIC

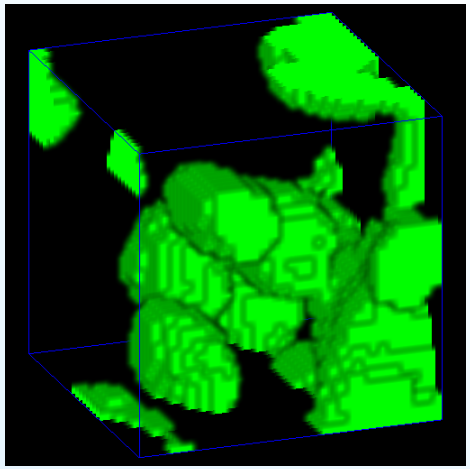

3D Squassh

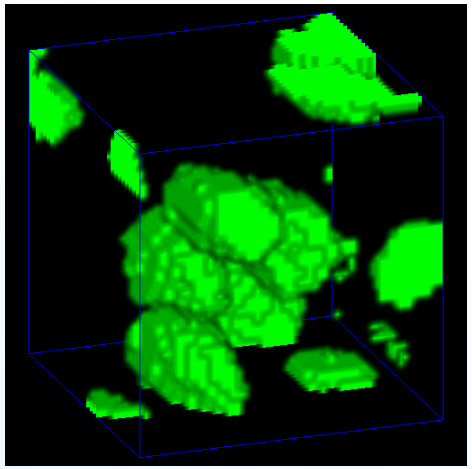

$2D^{+}$ CNN

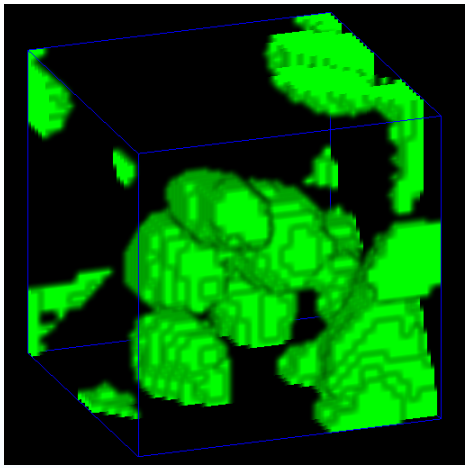

3D CNN

Volume 3 Result

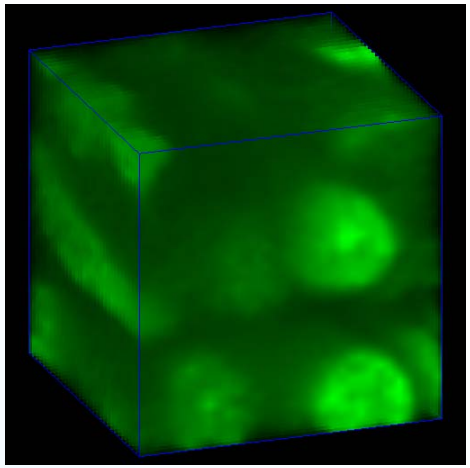

Original

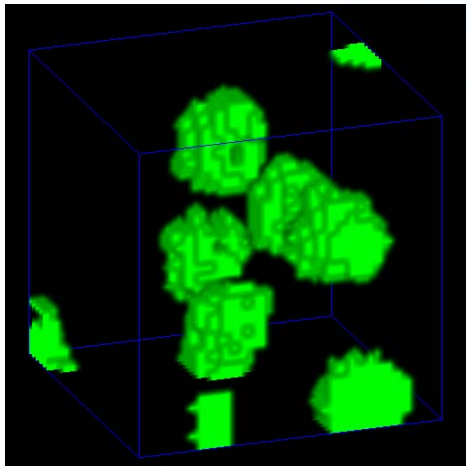

3D ground truth

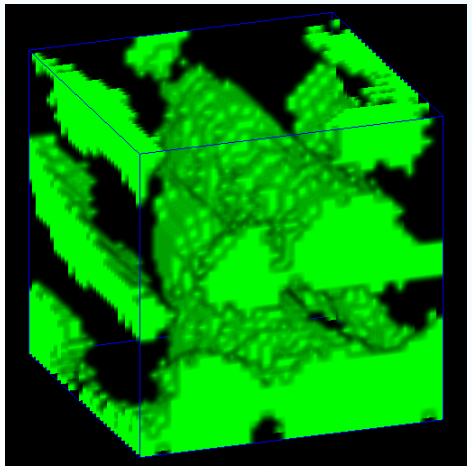

3Dac

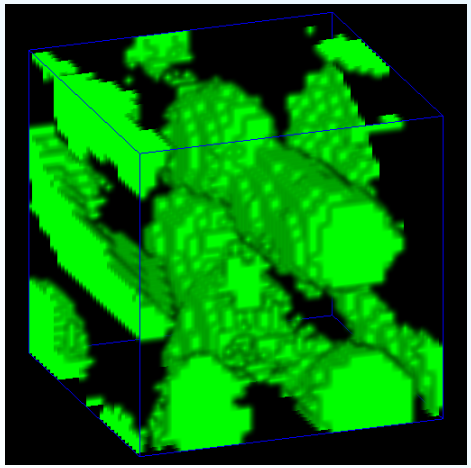

3DacIC

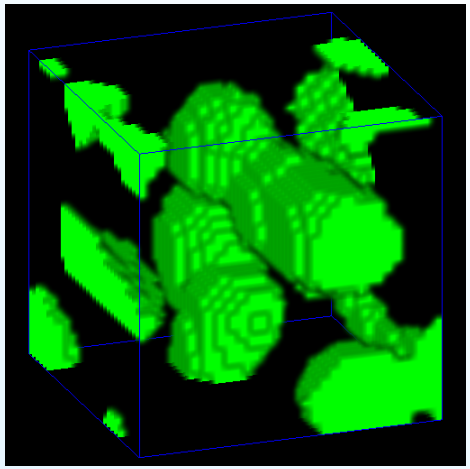

3D Squassh

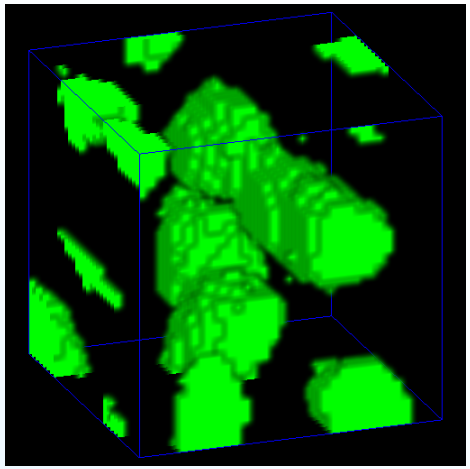

$2D^{+}$ CNN

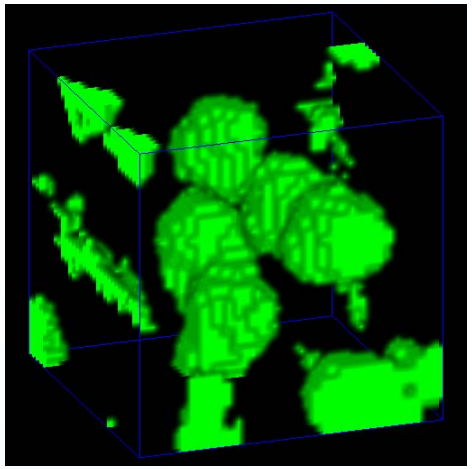

3D CNN

Tubule Boundary Segmentation

Jelly Filling

Jelly Filling Segmentation: Flowchart

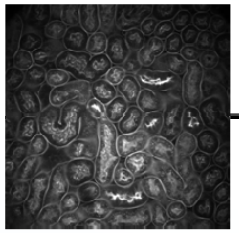

Original Image

Adaptive Thresholding

Initialize Tubule and Lumen Segmentation

All Images "*Done*"?

Yes

No

Result

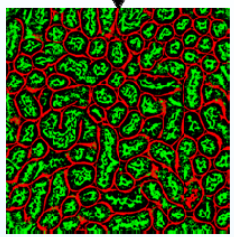

Initialize *p* (Image #) = 1

p = *p*+1

End Of Stack?

No

Yes

Background Labeling

Adjust Jelly Viscosity

Mark *p*th Image "*Done*"

Stopping Criterion Satisfied?

No

Yes

Obtain For Each Pixel:
Floating Component Potential
Motion-Compensated Z-Series Consistency Potential
Neighborhood Voting Potential
Total Segmentation Potential

Refine Segmentation

Jelly Filling Iterations: Illustration

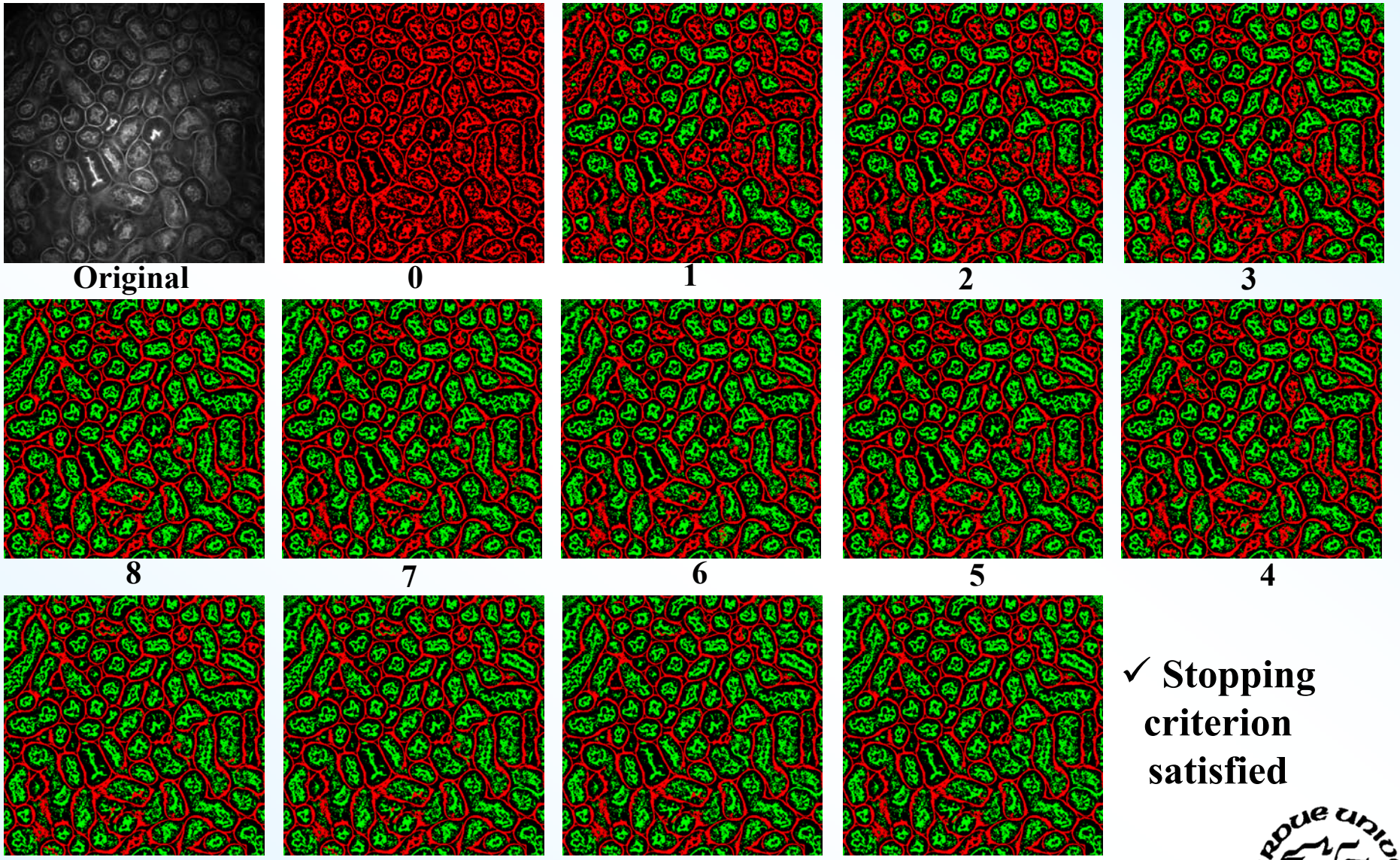

✓ Stopping criterion satisfied

Convergence Analysis

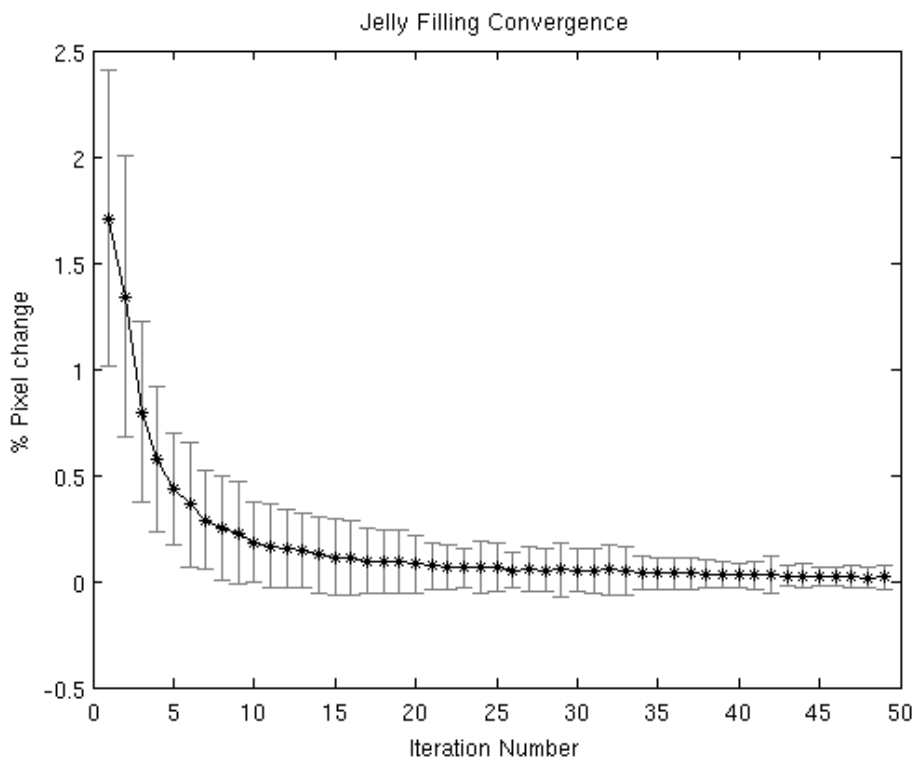

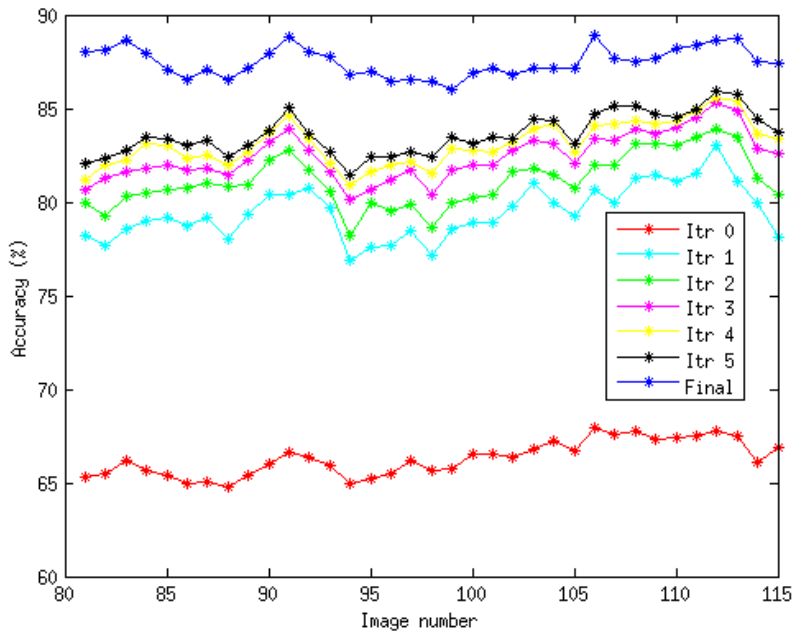

% Pixel Change Vs Jelly Filling Iterations

Segmentation Accuracy For Jelly Filling Iterations

Segmentation Results

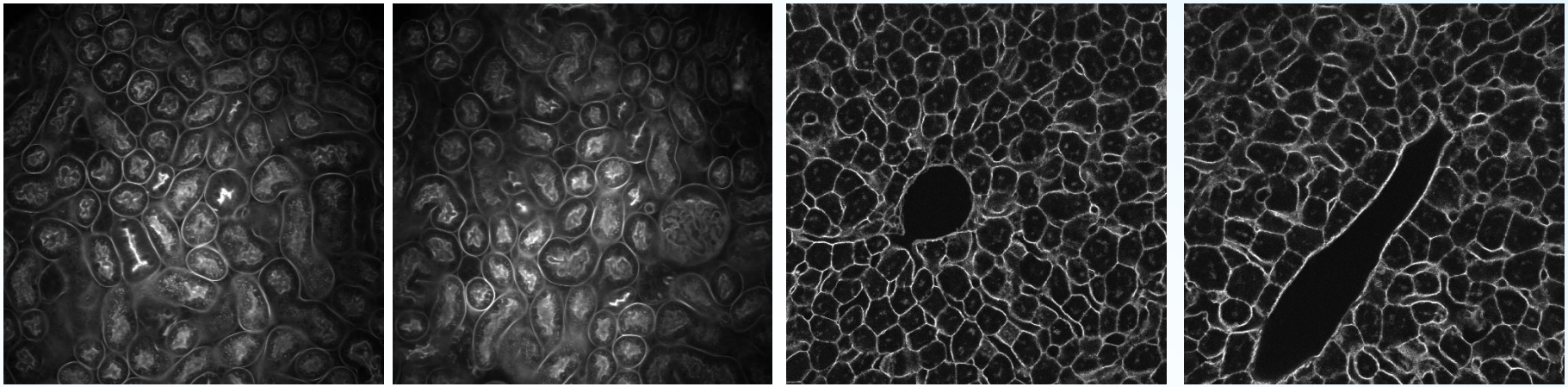

Kidney Original Images Liver

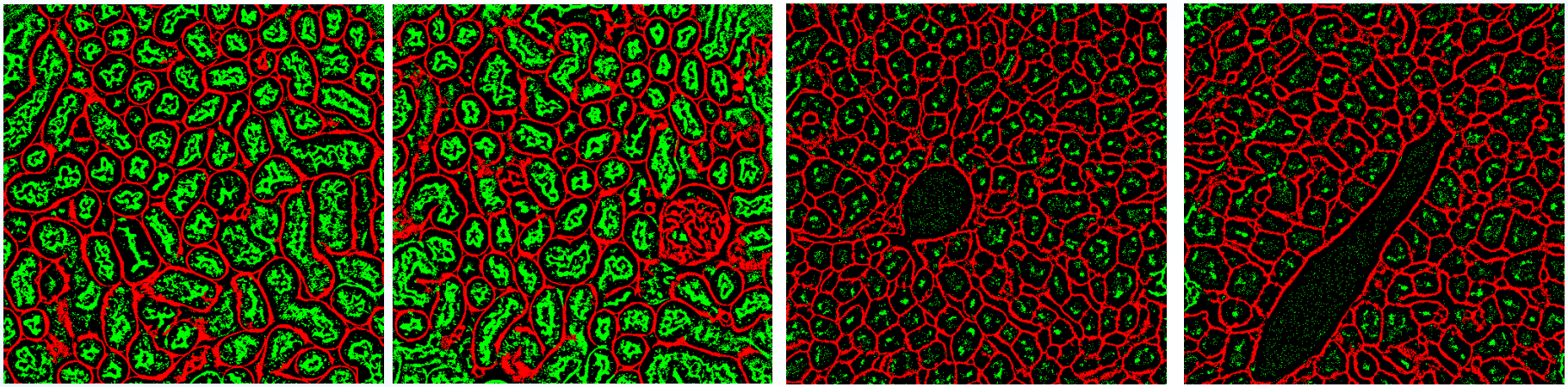

Segmentation Results

The kidney data was provided by Malgorzata Kamocka of Indiana University and was collected at the Indiana Center for Biological Microscopy and by Tarek Ashkar of the Indiana University Division of Nephrology. The liver data was provided by Sherry Clendenon and James Sluka of the Biocomplexity Institute, Indiana University at Bloomington.

Comparison With Other Work

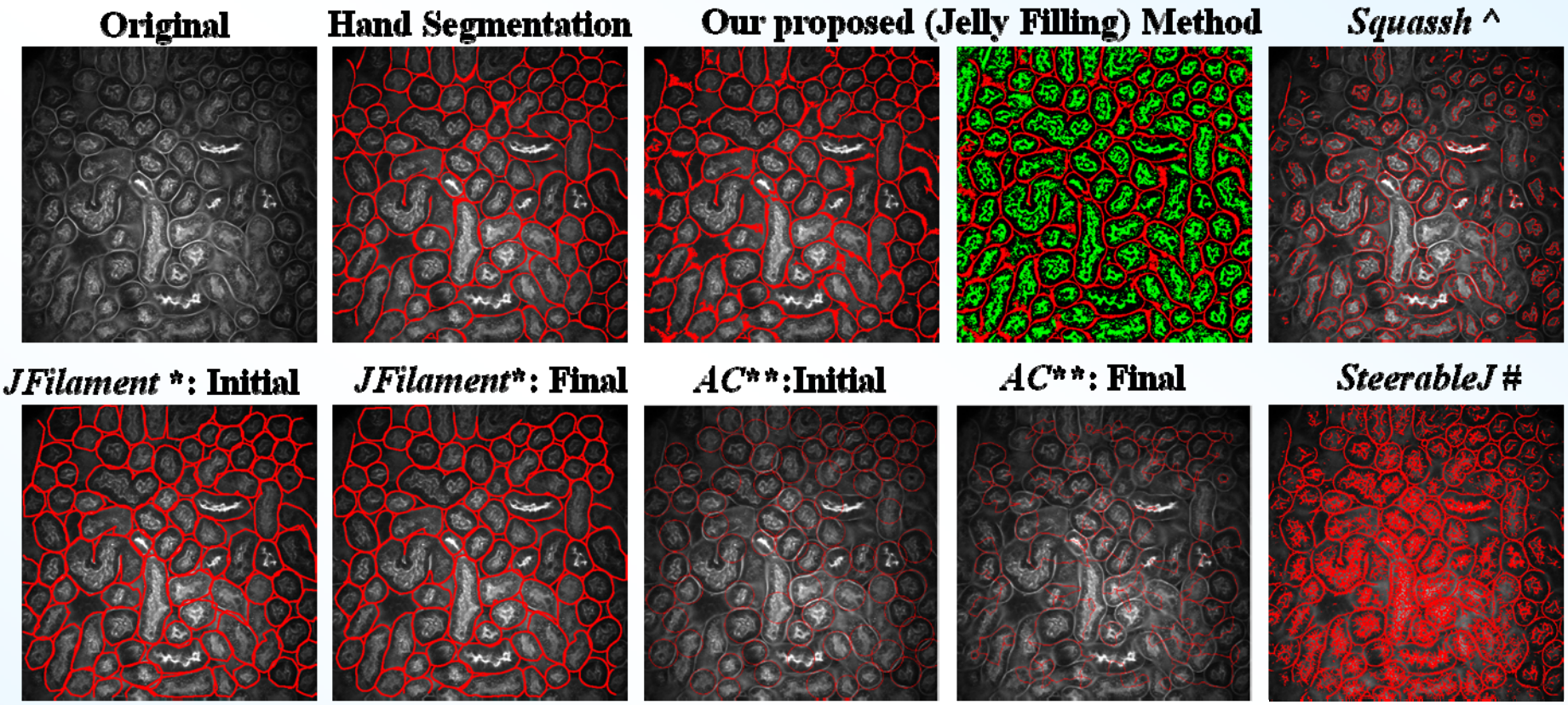

^ *Squassh:* G. Paul et. al, "Coupling image restoration and segmentation: A generalized linear model/Bregman perspective," International Journal of Computer Vision, vol. 104, no. 1, pp. 69–93, March 2013.

* *Jfilament*: H. Li et.al, "Automated actin filament segmentation, tracking and tip elongation measurements based on open active contour models," *Proceedings of the IEEE International Symposium on Biomedical Imaging*, pp. 1302–1305, June 2009, Boston, MA.

** *Active Contour* (*AC)*: B. Li, and S. Acton, "Active Contour External Force Using Vector Field Convolution for Image Segmentation," *IEEE Transactions on Image Processing*, vol. 16, no. 8, pp.2096-2106, August 2007

\# *SteerableJ:* M. Jacob and M. Unser, "Design of steerable filters for feature detection using Canny-like criteria," *IEEE Transactions on Pattern Analysis and Machine Intelligence*, vol. 26, no. 8, August 2004.

Comparison With Other Work

Method	Class	Accuracy	Type-I Error	Type-II Error	Comp. Time
Active Contour	SA	86.3%	2%	11.7%	50 min
JFilament	SA	90.4%	6.1%	3.5%	40 min
SteerableJ	A	72.4%	22.3%	5.3%	10 sec
3D Level Set	A	80.2%	8%	11.7%	10 sec
Squassh	A	83.5%	5.6%	11%	20 sec
Jelly Filling (proposed)	A	91.2%	6%	2.7%	80 sec

Example Kidney Image

Segmentation Results: 3D Visualization

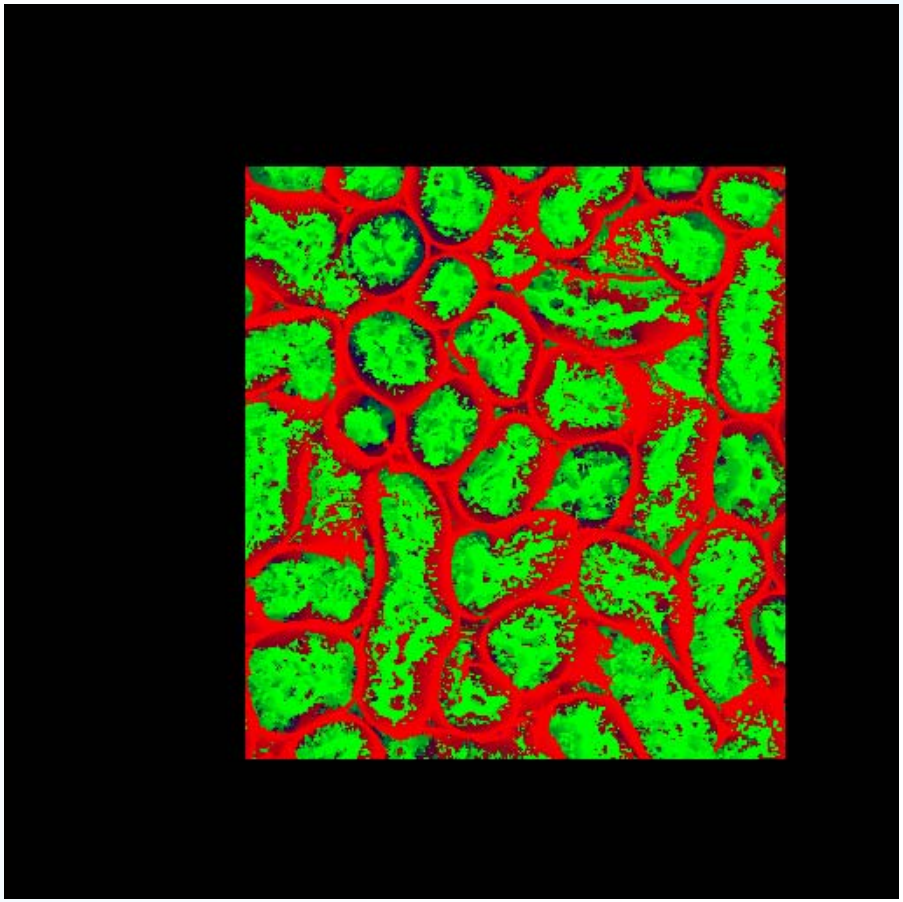

Kidney (Voxx v.2)

J. Clendenon et al., "Voxx: a PC-based, near real-time volume rendering system for biological microscopy," *American Journal of Physiology-Cell Physiology*, vol. 282, no. 1, pp. C213–C218, January 2002.

Future Work

- **Continue to investigate the use of machine learning methods particularly the use deep learning to segment biological structures in 3D**

- **Quantitative analysis (nuclei counting) by splitting segmented nuclei**

Recent Publications
(not complete)

- C. Fu, D. J. Ho, S. Han, P. Salama, K. W. Dunn, and E. J. Delp, "Nuclei Segmentation of Fluorescence Microscopy Images Using Convolutional Neural Networks," To appear, *Proceedings of the IEEE International Symposium on Biomedical Imaging* (*ISBI*), April 2017, Melbourne, Australia.
- S. Lee, P. Salama, K. W. Dunn, and E. J. Delp, "Segmentation of Fluorescence Microscopy Images Using Three Dimensional Active Contours with Inhomogeneity Correction," To appear, *Proceedings of the IEEE International Symposium on Biomedical Imaging* (*ISBI*), April 2017, Melbourne, Australia.
- D. J. Ho, P. Salama, K. W. Dunn, and E. J. Delp, "Boundary Segmentation for Fluorescence Microscopy Using Steerable Filters," *Proceedings of the SPIE Conference on Medical Imaging*, February 2017, Orlando, FL. DOI: 10.1117/12.2254627
- C. Fu, N. Gadgil, K. Tahboub, P. Salama, K. Dunn and E. J. Delp, "Four Dimensional Image Registration for Intravital Microscopy," *Proceedings of the Computer Vision for Microscopy Image Analysis* (*CVMI*) *workshop at Computer Vision and Pattern Recognition* (*CVPR*), July 2016, Las Vegas, NV. DOI: 10.1109/CVPRW.2016.175
- N. Gadgil, P. Salama, K. W. Dunn, and E. J. Delp, "Jelly Filling Segmentation of Fluorescence Microscopy Images Containing Incomplete Labeling," *Proceedings of the IEEE International Symposium on Biomedical Imaging* (*ISBI*), April 2016, Prague, Czech Republic. DOI: 10.1109/ISBI.2016.7493324
- N. Gadgil, P. Salama, K. W. Dunn, and E. J. Delp, "Nuclei Segmentation of Fluorescence Microscopy Images Based on Midpoint Analysis and Marked Point Process," *Proceedings of the IEEE Southwest Symposium on Image Analysis and Interpretation* (*SSIAI*), March 2016, Santa Fe, NM. DOI: 10.1109/SSIAI.2016.7459169